

Boletín Geológico, 48(1), 49-79, 2021.
[https://doi.org/10.32685/0120-1425/bol.
geol.48.1.2021.503](https://doi.org/10.32685/0120-1425/bol.geol.48.1.2021.503)



This work is distributed under the Creative
Commons Attribution 4.0 License.

Received: May 15, 2020

Revised: July 12, 2020

Accepted: October 9, 2020

Published online: July 12, 2021

San José de Guaviare Syenite, Colombia: Repeated Ediacaran intrusions in the northwestern Amazonian Craton

Sienita de San José de Guaviare, Colombia: Intrusiones
repetidas durante el Ediacárico en el noroeste del Cratón
Amazónico

Carolina Amaya López¹, Marion Weber Scharff², Mauricio Ibáñez Mejía³, Federico Alberto Cuadros Jiménez⁴, Jorge Julián Restrepo Álvarez¹, Nilson Francisquini Botelho⁴, Mario Maya Sánchez⁵, Orlando Manuel Pérez Parra⁶, Carlos Ramírez Cárdenas⁷

¹ Universidad Nacional de Colombia, Medellín, Colombia

² Departamento de Geociencias y Ambiente, Universidad Nacional de Colombia, Medellín, Colombia

³ Department of Earth and Environmental Sciences, University of Rochester, New York, USA

⁴ Instituto de Geosciências, Universidade de Brasília, Brazil

⁵ Servicio Geológico Colombiano, Bogotá, Colombia

⁶ Université Grenoble-Alpes, France

⁷ Faculty of Earth Sciences, Universitat de Barcelona-UB, Spain

Corresponding author: Carolina Amaya, caro.geologia@gmail.com

ABSTRACT

The Neoproterozoic igneous rocks found in the municipality of San José del Guaviare include several isolated plutonic bodies that protrude from the Phanerozoic sedimentary cover in belts aligned NW-SE. Limited to the Guaviare department, these intrusions stretch from the La Lindosa mountain range to the *corregimiento* El Capricho. These plutonic bodies consist of nepheline syenites, nepheline monzosyenites, nepheline-bearing alkali-feldspar syenites, syenites, quartz-syenites, quartz-alkali-feldspar syenites, syenogranites, and quartz-rich granitoids, which have been grouped and termed the San José de Guaviare Syenite unit (SJGS).

The intrusion of the unit occurred in the Ediacaran (604 ± 7 Ma and 620.5 ± 7.5 Ma) by mantle-derived alkaline magmas formed in anorogenic settings, most likely in rift-like stretching zones. The silica-subsaturated magma may have reacted with host rocks at the crust level, producing some silica-saturated igneous rocks, such as syenogranites and quartz-syenites, which are found in the El Capricho and Cerritos bodies.

Keywords: Nepheline Syenite, Neoproterozoic, Intraplate, Geochemistry, Geochronology.

Citation: Amaya L., C., Weber S., M., Ibáñez M., M., Cuadros, F. A., Restrepo A., J. J., Botelho, N. F., Maya S., M., Pérez P., O. M., & Ramírez C., C. (2021). San José de Guaviare Syenite, Colombia: Repeated Ediacaran intrusions in the northwestern Amazonian Craton. *Boletín Geológico*, 48(1), 49-79. <https://doi.org/10.32685/0120-1425/bol.geol.48.1.2021.503>

RESUMEN

Las rocas ígneas neoproterozoicas presentes en el municipio de San José del Guaviare están representadas por varios cuerpos plutónicos aislados que se extienden en franjas de sentido NW-SE y sobresalen de la cobertura sedimentaria fanerozoica. Restringidos al departamento de Guaviare, dichos intrusivos se extienden desde la serranía de La Lindosa hasta el corregimiento El Capricho. Estos cuerpos plutónicos están compuestos por sienitas nefelínicas, monzosienitas nefelínicas, sienitas de feldespato alcalino con nefelina, sienitas, cuarzosienitas, cuarzosienitas de feldespato alcalino, sienogranitos y granitoides ricos en cuarzo, que se agruparon en la unidad denominada Sienita de San José de Guaviare (SSJG).

La intrusión de esta unidad tuvo lugar en el Ediacárico (604 ± 7 Ma y $620,5 \pm 7,5$ Ma) a partir de magmas alcalinos que se formaron en ambientes anorogénicos manto-derivados, probablemente en zonas de distensión tipo *rift*. Este magma subsaturado en sílice habría reaccionado a nivel cortical con la roca encajante produciendo algunos magmas saturados en sílice, como los sienogranitos y cuarzosienitas que se presentan en los cuerpos El Capricho y Cerritos.

Palabras clave: Sienita nefelínica, Neoproterozoico, intraplaca, geoquímica, geocronología.

1. INTRODUCTION

The San José de Guaviare Syenite is located in eastern Colombia, in an area with exposed Precambrian plutonic igneous and metamorphic rocks, which belong to the crystalline basement of the NW Amazonian Craton. This unit forms several isolated bodies aligned NW, some of which are structurally controlled and related locally to Mesoproterozoic metamorphic rocks known as the Guaviare Complex (*Complejo Guaviare*), which shows contact metamorphism superimposed by the syenite intrusion (Maya et al., 2018).

Different studies have reported a total of four plutonic bodies (B) in the SJGS, of which the two northernmost bodies (La Pizarra B and Las Delicias B), located in La Lindosa mountain range, were identified and studied by Trumphy (1943, 1944), Gansser (1954), Pinson et al. (1962), Vesga and Castillo (1972), Galvis et al. (1979), and Arango et al. (2011, 2012). The two southernmost bodies (El Capricho B and Cerritos B), located near El Capricho corregimiento, have been explored in more recent studies such as those of Maya et al. (2018), Franco et al. (2018), and Muñoz Rocha et al. (2019).

Previous studies have focused on reporting Paleozoic or Precambrian syenite intrusive rocks located in the mountain range west of San José del Guaviare, Guaviare department, Colombia, belonging to the crystalline basement of the Amazonian Craton (Trumphy, 1943, 1944; Gansser, 1954; Pinson et al., 1962; Galvis et al., 1979). The most detailed early studies were performed by Vesga and Castillo (1972), followed by Arango et al. (2011, 2012). These authors focused on describing textures and structures and the petrography, geochemistry, and geochronology of

northern SJGS bodies. Other studies, such as those of Franco et al. (2018) and Muñoz Rocha et al. (2019), have complemented the age records of syenite rocks and their geochemistry.

In this study, southern syenite bodies were mapped at a 1:25000 scale (Maya et al., 2018), previously not possible for all bodies of the SJGS. We also studied their macroscopic and microscopic characteristics, geochemistry for major and trace elements, and U-Pb zircon geochronology. The existence of both feldspathoid and quartz rocks and the range of geochronological ages of the SJGS had not been previously reported. They will be essential to define the conditions under which events gave rise to the unit.

2. METHODS

2.1 Field geology and petrography

The field work was conducted in the Colombian Amazon region, between the municipalities of San José del Guaviare and El Retorno, in the Guaviare department, within the framework of the geologic mapping of Plate 372, El Retorno, performed by Serviminas S.A.S. from 2017 to 2019 for the Servicio Geológico Colombiano (SGC). The geological survey made use of the Instituto Geográfico Agustín Codazzi 1:25 000-scale topographic maps, following the parameters for collecting data in a field book established by Caicedo (2003) and updated by Serviminas S.A.S. (Maya et al., 2019). In total, 29 field stations were established in the SJGS, collecting 41 rocks samples of nepheline syenite, nepheline monzosyenite, quartz-syenite, syenite, sienogranite and hornfels, among others, of which 41 thin sections and two polished sections were prepared for analysis

by transmitted and reflected light microscopy, respectively, counting 300 points per sample. The composition and texture of the minerals were described according to Heinrich (1965), Bowie and Simpson (1977), and Winter (2001), and the rocks were classified based on their composition using the Quartz, Alkali feldspar, Plagioclase, Feldspathoid (QAPF) diagram of plutonic rocks by Streckeisen (1976).

The materials used and generated during this research, such as field maps, thin sections, polished sections, rock samples, and discards, have been deposited at the Servicio Geológico Colombiano, Bogotá headquarters.

2.2 Geochemistry

Geochemical analyses of major and trace elements, including rare-earth elements (REE), were performed by X-ray fluorescence (XRF) and by inductively coupled plasma mass spectrometry (ICP-MS), respectively, at ALS Global Ltd., in accordance with internal code specifications of the laboratory (ME-XRF26 and ME-MS81). The samples were crushed and pulverized to collect the < 200-mesh-size fraction. The analyses were performed following laboratory standards, including the melting of samples with LiBO₂ and acid digestion for ICP-MS.

2.3 Total-rock isotope analysis

Sm, Nd, and Sr isotope analyses were performed at the Geochronology and Isotope Geochemistry Laboratory of the University of Brasilia. The analytical procedures applied in this study to determine the ¹⁴⁷Sm/¹⁴⁴Nd and ¹⁴³Nd/¹⁴⁴Nd isotope ratios were those described by Gioia and Pimentel (2000). ¹⁴⁹Sm and ¹⁵⁰Nd spike solutions were added to the crushed and pulverized rock. Sm and Nd were separated on cation exchange columns. Two drops of 0.025 N H₃PO₄ were added to the resulting fractions, which were then evaporated. The residue was dissolved in 1 µl of 5% HNO₃ and mounted on a double Re filament on a Finnigan MAT 262 thermal ionization mass spectrometer with seven collectors in static mode. The uncertainties of the ¹⁴⁷Sm/¹⁴⁴Nd and ¹⁴³Nd/¹⁴⁴Nd isotope ratios were lower than 0.2% and 0.0033% (2σ), respectively, based on the analysis of the international standard BHVO-2. The ¹⁴³Nd/¹⁴⁴Nd ratio was normalized using a ¹⁴⁶Nd/¹⁴⁴Nd ratio = 0.7219 and a decay constant of 6.54 × 10⁻¹² a⁻¹ (Lugmair and Marti, 1978).

The procedures followed for Sr isotope analysis were those presented by Gioia et al. (1999). The samples were pulverized and subjected to acid dissolution and separation on cation

exchange columns. Subsequently, the Sr-containing fractions were deposited together with 1 µl of H₃PO₄ on a Ta filament in the mass spectrometer described above. Based on the analysis of the international standard NBS-987, the uncertainties of the ⁸⁷Sr/⁸⁶Sr ratio were lower than 0.0069% (2σ). The ⁸⁷Rb/⁸⁶Sr ratio was calculated based on the Rb and Sr concentrations of the samples assessed by ICP-MS (Annex 1), according to the procedure of Faure and Mensing (2005).

2.4 LA-ICP-MS U-Pb zircon geochronology

The samples were initially prepared at the EAFIT University (originally *Escuela de Administración, Finanzas e Instituto Tecnológico*), where zircon crystals were separated following standard crushing, sieving, and mineral concentration methods. Subsequently, at the University of Rochester, several crystals of each sample were mounted in epoxy resin and polished to expose an internal face, on which the textural and isotopic analyses were performed. Cathodoluminescence images, taken to reveal the internal structure of the study zircons and to guide the geochronological analyses, were acquired under a JEOL 7100FT field-emission scanning electron microscope with a Deben panchromatic cathodoluminescence detector at the Mackay Microbeam Laboratory, University of Nevada, Reno.

The U-Pb isotope analyses were performed at the University of Rochester on an Agilent 7900 ICP-MS coupled to a Photon Machine Analyte G2 laser ablation system. This contained a HelEx2 rapid purge cell and generated pulses lasting approximately 8 ns using an excited ArF excimer. During the analyses, the laser was operated at a repetition rate of 7 Hz and a spot size of 30-µm diameter, generating a constant energy density of approximately 7 J/cm² on the surface of the crystals. The ablations were conducted under an ultrahigh-purity He atmosphere, and the same gas was used to transport the ablation aerosol to the ICP-MS. Each analysis consisted of 15 s of an “analytical blank” measurement with the laser off, immediately followed by a 20-s measurement of the isotope composition of the crystals with the laser on. The isotopes ²⁰²Hg, ²⁰⁴(Pb+Hg), ²⁰⁶Pb, ²⁰⁷Pb, ²⁰⁸Pb, ²³²Th, and ²³⁸U were measured on the mass spectrometer. The instrumental bias was corrected using the standard-sample bracketing method with fragments of a Sri Lankan zircon (SL2) with a known age of 563.6 ± 3.2 Ma, assessed by isotope dilution thermal ionization mass spectrometry (ID-TIMS), as the primary reference material (Gehrels et al., 2008).

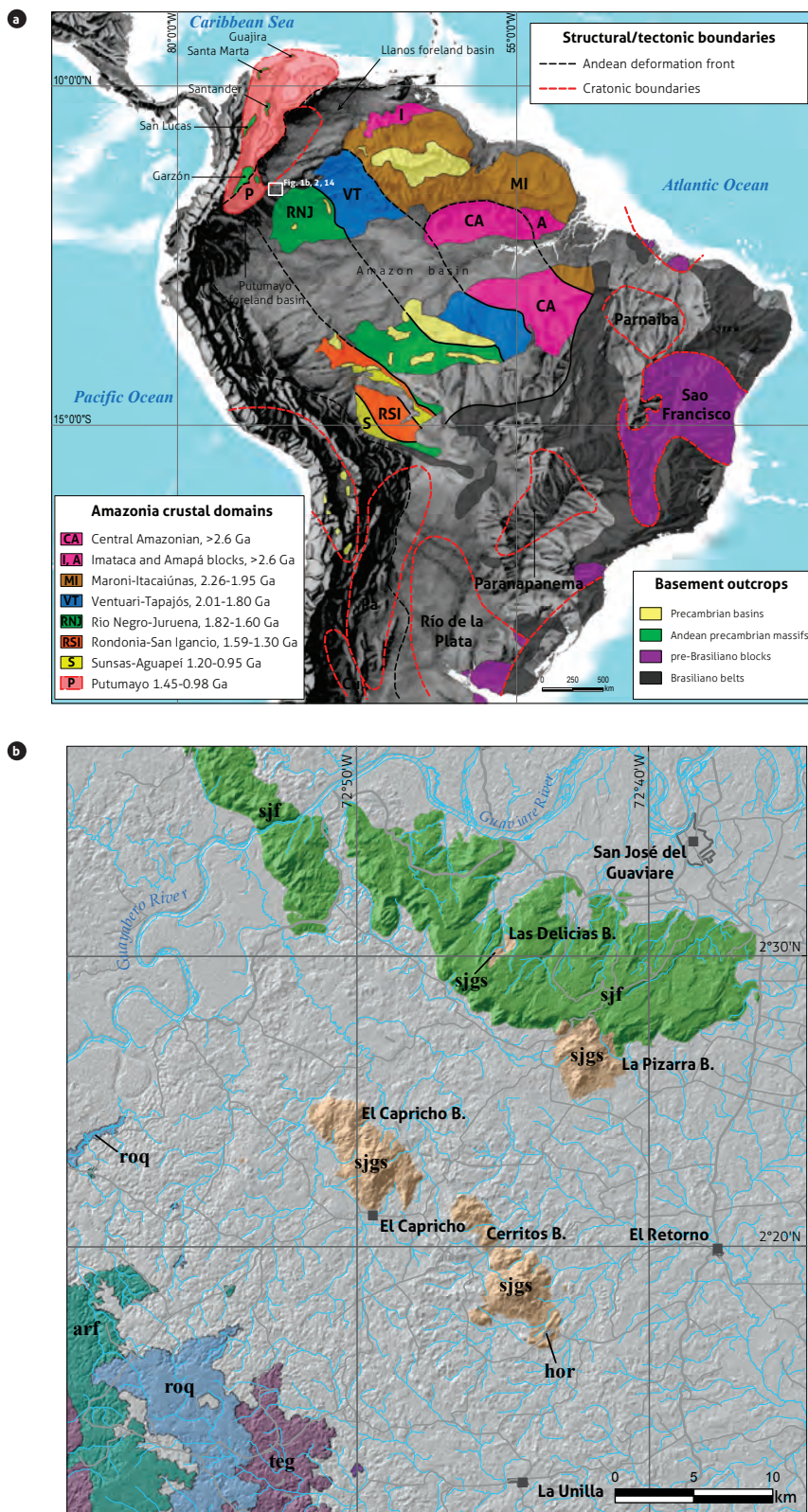


Figure 1. Map showing the locations of the syenite bodies and neighboring geological units teg: Termales Gneiss; roq: La Rompida Quartzite; sjgs: San José de Guaviare Syenite; arf: Araracuara Formation; sjf: San José Formation. Source: adapted from Nivia et al. (2011), Maya et al. (2018), and Ibáñez Mejía and Cordani (2019).

U-Pb data were processed using the procedures and algorithms described by Pullen et al. (2018) to make the necessary linearity corrections of the detection system. In addition to the primary reference material and to zircons from the San José de Guaviare Syenite, during our analytical session, several Plešovice and FC-1 zircon fragments (Duluth Gabbro Complex, Minnesota) were also analyzed to assess the precision, accuracy, and reproducibility of the method. Said secondary materials yielded weighted average ages of $^{206}\text{Pb}/^{238}\text{U}=335.0 \pm 1.2/3.9$ (2σ , $n=21$, $\text{MSWD}=0.8$) for Plešovice and $^{207}\text{Pb}/^{206}\text{Pb}=1098 \pm 8/11$ (2σ , $n=23$, $\text{MSWD}=0.3$) for FC-1 zircons. The first level of uncertainty reported represents only internal analytical uncertainties, and the second level of uncertainty includes the propagation of systematic uncertainty and standardization sources. By including the systematic uncertainties, the values assessed in our analytical session become indistinguishable from the reference ages of 337.13 ± 0.37 Ma for Plešovice (Sláma et al., 2008) and 1099.96 ± 0.58 Ma for FC-1 (Ibáñez-Mejía and Tissot, 2019), determined by CA-ID-TIMS, which confirms that the geochronological results reported in this study are accurate and that the analytical uncertainties have been correctly assigned.

3. GEOLOGICAL FRAMEWORK

The SJGS represents a period of tectonism-related intrusions after the Precambrian bodies of the Amazonian Craton basement (Pinson et al., 1962; Vesga and Castillo, 1972), and this magmatic event was the last relevant igneous activity that occurred in the western section of the Amazonian craton (Galvis et al., 1979).

According to the K-Ar and Rb-Sr biotite ages assessed by Pinson et al. (1962), these rocks would be Paleozoic, dated between the Early Ordovician and the Late Ordovician, with different episodes of intrusion, although the K-Ar and Rb-Sr biotite dating methods used actually indicate a cooling below approximately 300 °C. Toussaint (1993) indicates that the nepheline syenite bodies correspond to the last early Paleozoic magmatism of the Autochthonous Block (*Bloque Autóctono*), resulting from local partial melting of the base of the continental crust of the Eastern Range (*Llanos Orientales*), which would have been affected by a stretching movement that increased the thermal flow in the region.

Nevertheless, the U-Pb zircon age assessed by Arango et al. (2012) dated the unit to the Ediacaran (Neoproterozoic), with a proposed origin from anatexis processes of migmatitic metamorphic rocks, which are related to the Pan-African event

during the Cambrian in the continent Gondwana. The U-Pb ages assessed in the study conducted by Franco et al. (2018) are similar, but the authors diverge in their interpretation of the origin of these rocks, which indicates that the intraplate alkaline magmatism of the Neoproterozoic-Cambrian, east of Colombia and absent from the Colombian Andes, could have derived from Pan-African orogeny during the accretion of mobile belts in the NW continental margin of Gondwana.

The SJGS rocks are overlaid by sedimentary formations deposited in unconformity over the unit, such as the San José Formation from the Cretaceous (Figure 1) (Arango et al., 2011, 2012) and the Caja Formation from the Neogene (Maya et al., 2018). Furthermore, in the southern section of the Cerritos body, the SJGS is in contact with Proterozoic metamorphic rocks (Maya et al., 2018), where igneous rocks intrude into metamorphic rocks, creating a thermal effect, evidenced in the recrystallization to hornfels and in the formation of injection migmatites. Approximately 6 km west of the El Capricho body, a small syenite outcrop (Figure 2) shows that the extent of the unit is mostly under the sedimentary cover.

Approximately 15 km southwest of the syenite bodies, basement rocks, named the Guaviare Complex by Maya et al. (2018) (Termales Gneiss and La Rompida Quartzite), as well as the Araracuara Formation (Figure 1) crop out, and there are no other syenite bodies in this section.

4. RESULTS

4.1 Lithology

The San José de Guaviare Syenite, in the southern section, encompasses two bodies aligned NW-SE located in the El Capricho and Cerritos sectors (Figure 2). In general, these bodies correspond to holocrystalline, phaneritic, hypidiomorphic rocks, ranging from equigranular (Figure 3A) to inequigranular. They are leucocratic, with a medium to coarse grain size, up to pegmatitic (7 cm) (Figure 3B), with a low to medium color index (7-20%) and with white, gray, and pink hues mottled with black. The El Capricho body is the most homogeneous in both composition and texture. The Cerritos body tends to be heterogeneous, with locally dark-gray fine-grained facies, which preserve the mineralogical composition, as well as rocks oriented by a mafic mineral flow (Figure 3 A, C).

In the southern section of the Cerritos body, SJGS intrusion generated a contact aureole in the regional metamorphic rocks of the Guaviare Complex, forming hornfels covering an area of

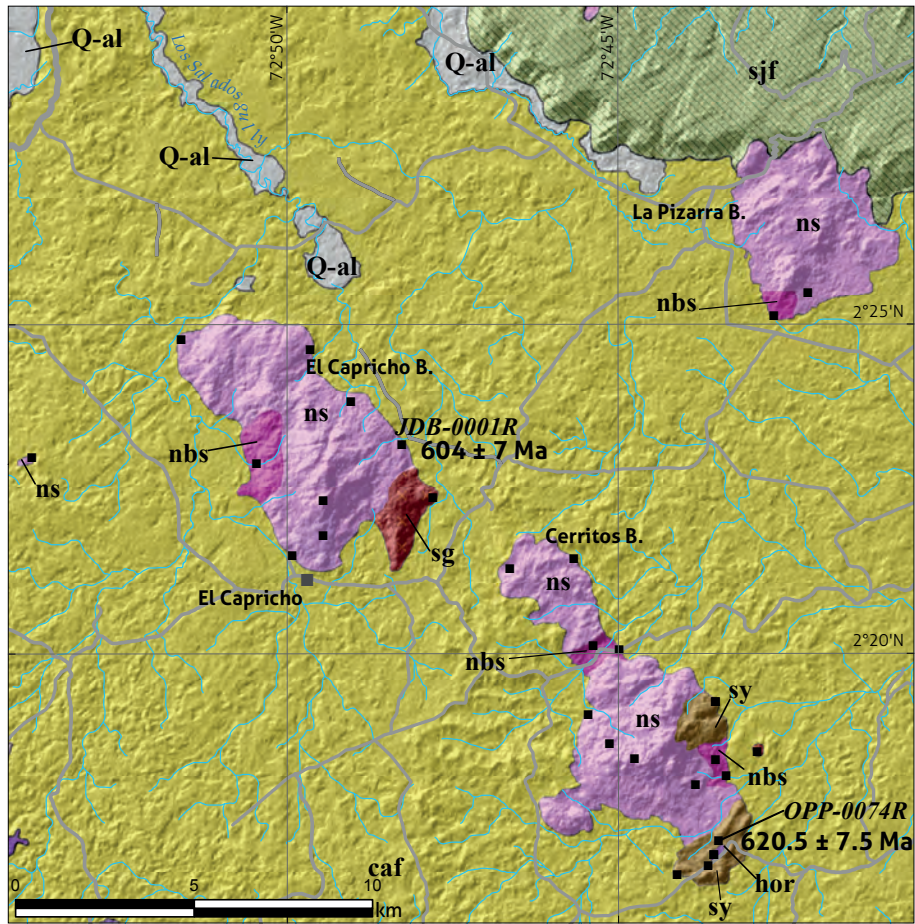


Figure 2. SJGS compositional distribution

ns: nepheline syenite; nbs: nepheline-bearing alkali-feldspar syenite; sg: syenogranite; sy: syenite; hor: hornfels; sjf: San José Formation; caf: Caja Formation; Q-al: alluvial deposits; ■: samples.

0.1 km². Although this type of rock only crops out in this zone, it provides considerable information about the origin of the syenites. The hornfels have a fine to medium grain, with black, gray, and red hues, some of which show banding and vestiges of the original orientation of the rock. At the same place, the rocks show silicification and form injection migmatites (Figure 3D), with stromatic textures. They are also characterized by the presence of syenite dikes, intersecting the injection migmatites and enveloping hornfels xenoliths.

4.2 Petrography

4.2.1 Syenites

San José de Guaviare syenite comprises mostly rocks with nepheline-like feldspathoids (Annex 2). Unlike the northern bodies, described by Arango et al. (2011, 2012), the southern

bodies contain quartz (Figure 4). The nepheline-bearing rocks are petrographically classified according to Streckeisen (1976) into nepheline syenite, nepheline monzosyenite, and nepheline-bearing alkali-feldspar syenite (Figures 4 and 5a). Two lithological facies are recognized in these rocks (Figure 2): one with a nepheline content higher than 15.7% (facies 1-F1) and another impoverished in nepheline, with amounts lower than 11.0% (facies 2-F2). Two samples analyzed in this study, collected in the southernmost section of the La Pizarra body, in the El Turpial sector, are also nepheline-bearing lithological facies.

The rocks with quartz correspond to syenogranite, syenite, quartz-syenite, and quartz-alkali feldspar syenite (Figure 4). According to the quartz content, two facies are differentiated (Figure 2): facies 3 (F3) is rich in quartz (>19.4%), and facies 4 (F4) is impoverished in it (<9.3%). Both facies are characteri-

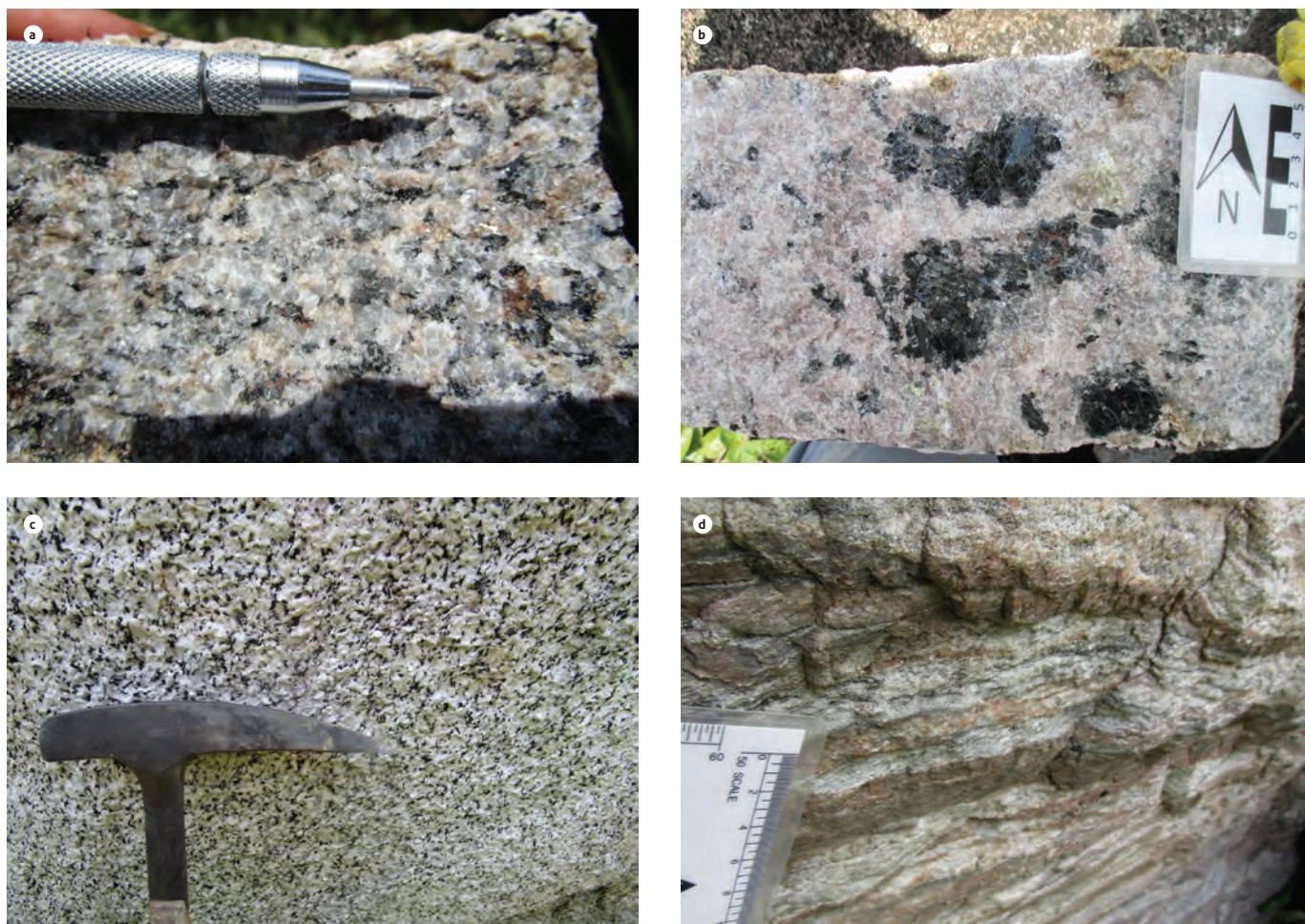


Figure 3. Texture and lithology of macroscopic samples from the SJGS a) Equigranular, medium grain, slightly oriented; b) Pegmatitic biotite crystals; c) Slight orientation through mafic mineral flow; d) Injection migmatites.

zed by the occurrence of arfvedsonite-like amphibole (Figure 5b). The zone of contact between the SJGS and metamorphic rocks of the Guaviare Complex shows silicification ($Qz > 68\%$), most likely through host rock assimilation; this sample was classified as a quartz-rich granitoid (Figure 4).

In general, these rocks have a holocrystalline, hypidiomorphic, inequigranular to equigranular texture, with a medium to coarse grain. Some samples show mineral orientation, defined by biotite, and others show recrystallization with a polygonal granoblastic texture (Figure 5c). Mineralogically, they consist of microcline, plagioclase, nepheline or quartz, biotite, arfvedsonite, and aegirine.

Microcline presents as subhedral to anhedral, tabular crystals with gridiron and Carlsbad twinning, which implies formation from orthoclase. Sometimes the microcline forms an

exsolution (perthite and mesoperthite) and myrmekitic fan texture, with plagioclase, nepheline, biotite, and calcite inclusions, and is slightly altered to clays and sericite. Albite to oligoclase plagioclase, determined using the Michel-Levy method, forms individual subhedral to euhedral, tabular, zoned crystals with albite, albite-Carlsbad, and Carlsbad twinning and with mesoperthitic and anti-perthitic textures, along with wedge-shaped lamellae and with calcite and biotite inclusions, sometimes altered to sericite and recrystallized along the grain boundaries, which causes the loss of extinction that is characteristic of this mineral.

Nepheline is found in subhedral to euhedral crystals with shapes ranging from rectangular to hexagonal, with simple twinned crystals and microcline, plagioclase, biotite, and calcite inclusions in poikilitic textures, showing slight alteration to

sericite, cancrinite, and natrolite. Quartz is found in colorless, clean, uniformly distributed anhedral crystals with undulose extinction, forming granular mosaics of complete contact with microcline and plagioclase.

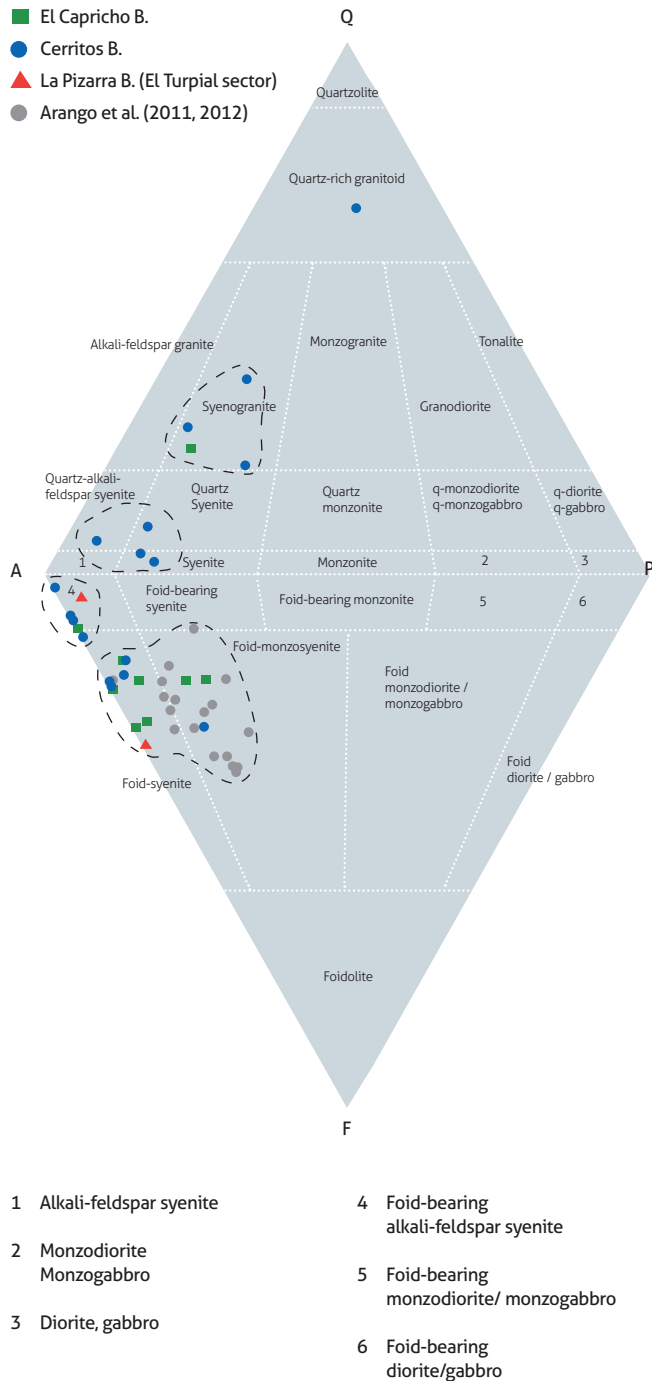


Figure 4. Classification of the SJGS samples in the QAPF diagram (Streckeisen, 1976)

Biotite is found in subhedral to euhedral, tabular crystals with strong pleochroism with X(α): pale yellowish brown, Y(β)=Z(γ): dark reddish or greenish brown, simple twinning, and bird's eye and undulose extinction. Sometimes the biotite shows a preferential orientation in undeformed clustered laths, which is therefore interpreted as the flow orientation. Some crystals have pleochroic halos around inclusions of zircon, while others are embayed, skeletal crystals, and they are replaced by muscovite, sericite, and chlorite along the grain boundaries.

Arfvedsonite amphibole forms subhedral to anhedral, columnar to hexagonal crystals, with simple twinning and strong pleochroism with X(α): bluish green, Y(β): greenish brown, and Z(γ): olive green, in columnar aggregates with biotite, titanite, and zircon. It is replaced by biotite towards the edges and fractures. Pyroxene-like aegirine is found in short, columnar, subhedral to anhedral crystals with strong pleochroism with X(α): dark green, Z(γ): brownish yellow, and Y(β): green. Aegirine is associated with arfvedsonite through possible transformation to amphibole. Cleavage planes are filled by opaque minerals possibly due to oxidation.

The primary accessory minerals correspond to granular opaque minerals, with sharp rhombic, square shapes or with skeletal textures, which correspond to pyrite and magnetite/ilmenite, in addition to titanite with simple twinning, some fractured and overgrown zircons, calcite-like carbonate, epidote, apatite, tourmaline, allanite, pyrochlore, and garnet, possibly melanite. Franco et al. (2018) mention that the syenites contain large magmatic zircons with a partly metamictic character.

Secondary accessory minerals, such as cancrinite, sericite, and natrolite, result from the alteration of nepheline in the cleavage planes, edges, and fractures of the host mineral. Sericite aggregates with carbonates are also an alteration product from the interior and edges of microcline, plagioclase, and biotite crystals.

4.2.2 Hornfels

The different types of hornfels identified by petrographic analysis highlight how the compositional variation of the host rock was affected by thermal metamorphism during the SJGS intrusion. Thus, pelitic and mafic protolith hornfels were initially subjected to regional metamorphism within the Guaviare Complex and later to thermal metamorphism in amphibolite facies (previously hornblende hornfels) and pyroxene hornfels. In addition, feldspar-quartz hornfels correspond to a syenite

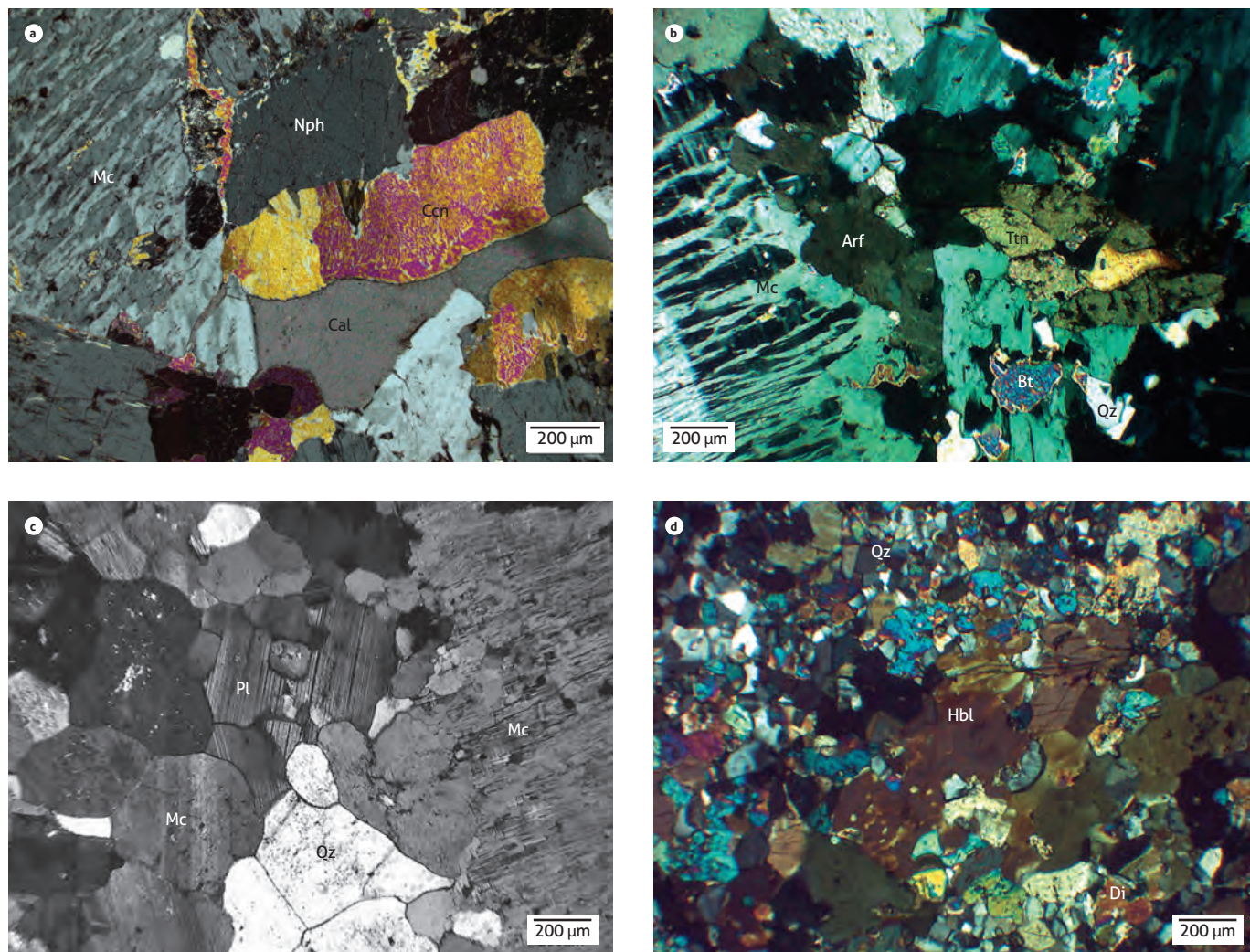


Figure 5. Mineralogy and textures of SJGS rocks

a) Nepheline (Nph)-, microcline (Mc)-, cancrinite (Ccn)-, and calcite (Cal)-bearing, hypidiomorphic, holocrystalline nepheline syenite; b) Syenite with aggregates of arfvedsonite (Arf), titanite (Ttn), and biotite (Bt); c) Syenite with recrystallized zone in polygonal granoblastic mosaics with straight edges of plagioclase (Pl), quartz (Qz), and microcline (Mc); d) Mafic hornfels with quartz-feldspathic domains and mafic domains (Di: diopside; Hbl: hornblende).

material recrystallized through intrusive processes, which occurred at various stages during the period of magmatism that originated the SJGS, as also shown by the wide range of ages assessed by geochronology and the many multielement and REE patterns found in geochemistry.

These rocks have a polygonal granoblastic texture and occasionally relict orientation derived from the original rock. The feldspar-quartz hornfels mineralogically consist of microcline, plagioclase, quartz, biotite, muscovite, and epidote (Annex 2), with zircon, calcite, apatite, titanite, fluorite, and opaque minerals as accessory minerals. The pelitic hornfels have

a similar composition to that of feldspar-quartz hornfels but contain andalusite and sillimanite. The mafic hornfels (Figure 5d) show banding with mafic and quartz feldspar domains, compositionally differing in the occurrence of hornblende and clinopyroxene.

Quartz is detected as xenoblast crystals, with undulose extinction and granoblastic to polygonal texture. Microcline is identified as subidioblastic to xenoblastic, tabular crystals with gridiron twinning and slight sericitization. Albite and oligoclase plagioclase, as determined using the Michel-Levy method, ranges from subidioblastic to idioblastic and is tabular,

with albite twinning, apatite inclusions, and slight alteration to saussurite. Biotite ranges from subidioblastic to idioblastic and is laminar with strong pleochroism, X(α): very pale yellow to Y(β)=Z(γ): dark brown, some with mimetic orientation, whereas others are disordered. Occasionally, they exhibit irregular boundaries and moderate chloritization. Muscovite is identified as xenoblastic to subidioblastic, laminar crystals with irregular boundaries and without any orientation, in intergrowths of biotite.

Hornblende is subidioblastic, columnar, with strong pleochroism X(α): pale yellow, Z(γ): dark green, Y(β): greenish yellow, forming aggregates with titanite. Clinopyroxene (diopside) is found associated with hornblende in xenoblasts with slight pleochroism X(α): pale bluish green, Z(γ): pale brownish green, Y(β): pale brownish yellow. Hornblende appears to replace clinopyroxene, most likely due to retrogression. Epidote is associated with biotite, suggesting epidotization, whereas zircon is found in inclusions, forming pleochroic halos in biotite. The opaque minerals are identified as pyrite, ilmenite, and magnetite.

4.3 Geochemistry

Eighteen representative samples of the petrographic groups were selected to analyze major, minor, and trace elements (Annex 1). The rocks from the San José de Guaviare Syenite are classified as nepheline syenites, syenites, and granites, according to the classification diagram of plutonic rocks by Cox et al. (1979) (Figure 6). They were subdivided into three groups according to their major and trace elements. In general, the rocks are peralkaline, according to the alkalinity index by Maniar and Piccoli (1989), but some rocks are placed in the metaluminous (group 3, mainly) or peraluminous (group 2) fields (Figure 7).

The samples included in group 1 are classified as nepheline syenites (Figure 6) and characterized by their low SiO₂ (53.58-55.40%), CaO (0.44-1.04%), MgO (0.21-0.80%), and P₂O₅ (0.01-0.04%) and high Al₂O₃ (20.08-22.81%) and Na₂O contents (7.51-8.98%). These samples have a lower Zr content (61-259 ppm) than the samples from groups 2 and 3 (134-4070 ppm).

The samples from group 2 are mostly classified as nepheline syenites, one of which is classified as syenite (Figure 6). They show a higher SiO₂ content than those of group 1 (56.35-63.86%) and are characterized by their low CaO (0.04-0.49%), MgO (0.03-0.46%), and P₂O₅ (<0.01-0.09%) and high Al₂O₃ (18.53-22.76%) and Na₂O contents (6.10-9.56%).

Some samples have abnormally high concentrations of Zr (4070 and 1970 ppm). These values may be related to the abundance of zircon. In this group, the high Nb content is also notable (up to 625 ppm in sample JDB-0011R), which can be explained by the presence of trace pyrochlore contents in the rock. The rocks of groups 1 and 2 are generally impoverished in TiO₂, and the samples from group 2 have a very low modal proportion or do not contain titanite in their mineralogy, in contrast to those from groups 1 and 3.

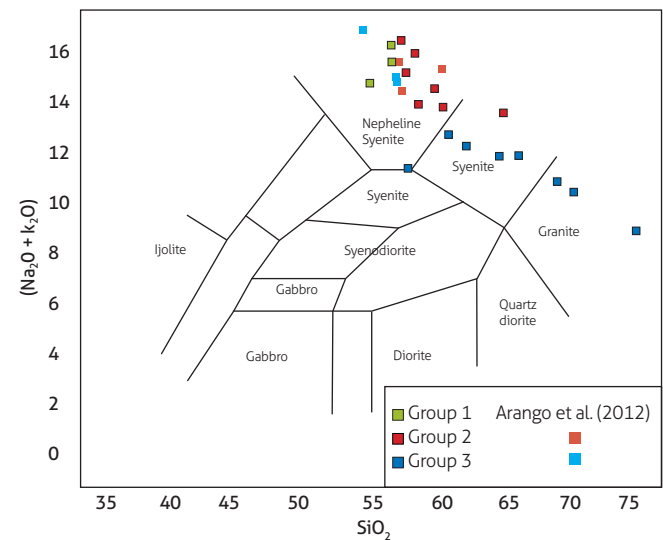


Figure 6. Total alkali-silica (TAS) diagram (Cox et al., 1979) of SJGS rocks, divided into three compositional groups

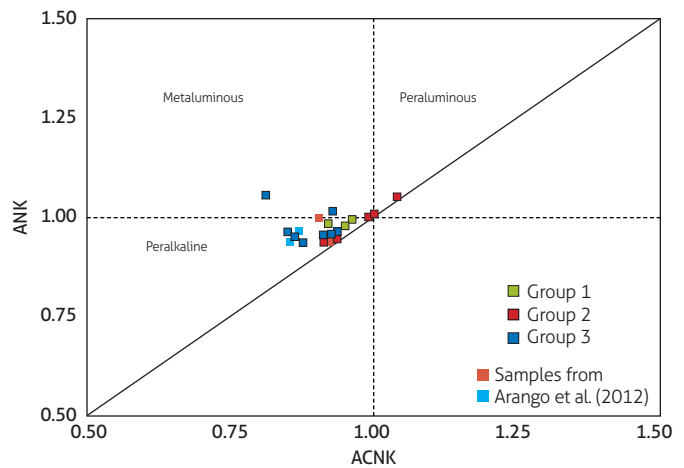


Figure 7. Alkalinity index (Maniar and Piccoli, 1989) of SJGS rocks. The rock samples mainly belong to the peralkaline field.

The samples associated with group 3 include rocks saturated and subsaturated with SiO₂ (56.31-74.20%). They are mainly classified as syenites and granites (Figure 6). In contrast to the rocks from the two previous groups, these rocks are impoverished in Al₂O₃ (12.63-18.53%) and Na₂O (3.30-6.63%) and enriched in CaO (0.26-3.60%), MgO (0.13-1.82%), and P₂O₅ (0.02-0.53%).

When graphed on primitive mantle-normalized multielement diagrams (McDonough et al., 1992) (Figure 8), group 1 is homogeneous, showing negative U, Th, and light rare-earth elements (LREE) anomalies and a slightly positive Sr anomaly. Group 2 is heterogeneous and shows a pointed pattern, with

negative Ba anomalies and positive U, K, Sr, and Zr anomalies in some samples. Group 3 shows a relatively coherent pattern, with negative Sr and Ti anomalies and with some variability in elements such as Ba, Th, U, and LREE.

In chondrite-normalized REE patterns (Figure 8), group 1 shows enrichment in LREE over middle (MREE) and heavy rare-earth elements (HREE), and the slope of the curve is relatively gentle (La/Yb)_N=19.2-23.2. Group 2 displays a “reverse spoon” pattern, showing a relative impoverishment in MREE [(La/Sm)_N=4.0-11.1 (Sm/Yb)_N=0.2-2.9] compared to LREE and HREE; some samples show a slight (CAL-0023R and CAL-0017R) to strong positive Eu anomaly (ENA-0036R), which

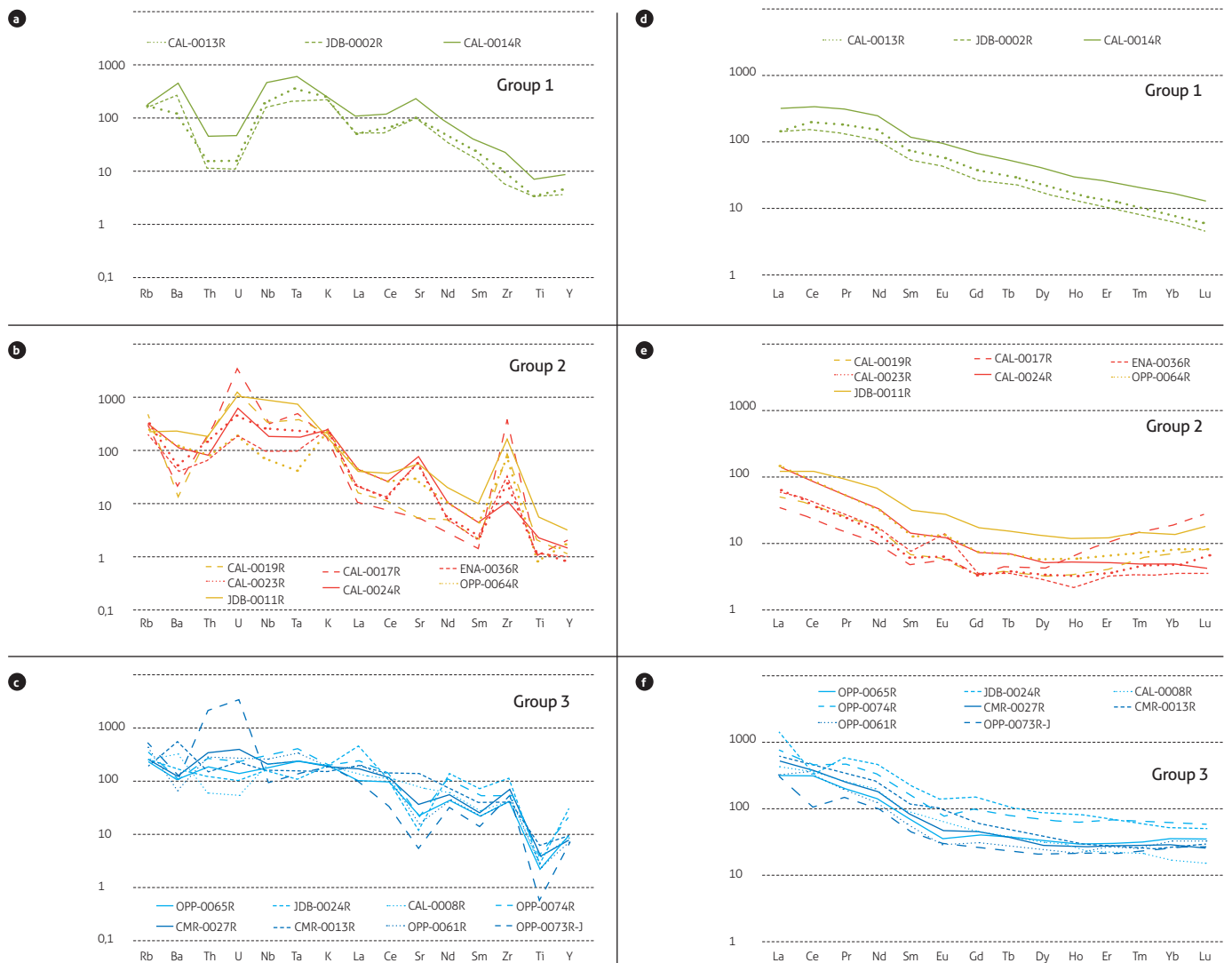


Figure 8. Primitive mantle- (McDonough et al., 1992) (a, b and c) and chondrite- (McDonough and Sun, 1995) (d, e and f) normalized multielement diagrams of SJS rocks

indicates a possible plagioclase accumulation during the magmatic history or the inheritance of this pattern from the original source. Group 3 is less homogeneous than the other groups and shows an enrichment in LREE in relation to HREE, with a relatively gentle slope $[(La/Yb)_N=8.9 - 28.0]$; these samples show a negative Eu anomaly, except two samples (CAL-0008R and CMR-0013R) had a slightly positive Eu anomaly. Most likely, the REE patterns reflect early differentiation of titanite and consequent loss of these magmatic elements.

The phase diagram of the $NaAlSiO_4$ - $KAlSiO_4$ - SiO_2 system (Hamilton and Mackenzie, 1965) (Figure 9) shows that the Si-subsaturated rocks of the San José de Guaviare Syenite are defined by a crystallization sequence in which, once the temperature decreases, two pathways occur: one in which nepheline crystallizes first, and another in which potassium feldspar crystallizes first, as shown by the textural relationships of euhedral nepheline inclusions in feldspar crystals, whereas other samples exhibit feldspar crystals in nepheline. In both cases, the residual liquid corresponds to nepheline syenite magma.

Si-saturated magmas (especially in group 3), which are found at the top of the Ab-Or line, when the temperature decreases, initially crystallize alkali feldspar or quartz. As the temperature decreases, the liquid increases or decreases in Si. The final outcome of the fractionation corresponds to granite magma. These paths are reflected in granitic rocks in which quartz is the last crystallization phase.

Rocks with intermediate compositions between both compositions, which correspond to syenites, should tend towards either of the previous two during the fractional crystallization process, meaning the abundance of these rocks results from magma mixing (Storey et al., 1989), assimilation of continental crust (Motoki et al., 2010), or absorption of previously precipitated cumulus feldspar material by new magma inside the magma chamber (Wolff, 2017).

The Silica Saturation Index (SSI) vs. $(K^+Na)/Al$ diagram (Figure 10a) shows that the rocks from groups 1 and 2 are classified as alkaline rocks, whereas the rocks from group 3 primarily belong to the nonalkaline field. In general, the samples define a linear pattern, especially those of group 3, in which $(K^+Na)/Al$ does not decrease when transitioning from a SiO_2 -subsaturated ($SSI < 0$) to a SiO_2 -saturated ($SSI > 0$) magma, which indicates crust assimilation, possibly alkaline. The patterns observed in the Rb/K vs. Nb/Y diagram (Figure 10b) suggest that the samples from group 1 are the least evolved and the closest to the original composition of the magma and that the samples from groups 2 and 3 were mainly formed by fractional crystallization and assimilation of continental crust, respectively.

The fractioning of titanite and zircon is noticeable in the diagrams of Figure 10c, d, e, in which the samples of the three groups are clearly separated. The anomalies observed in the REE patterns are also expressed in the diagrams of Figure 10f,

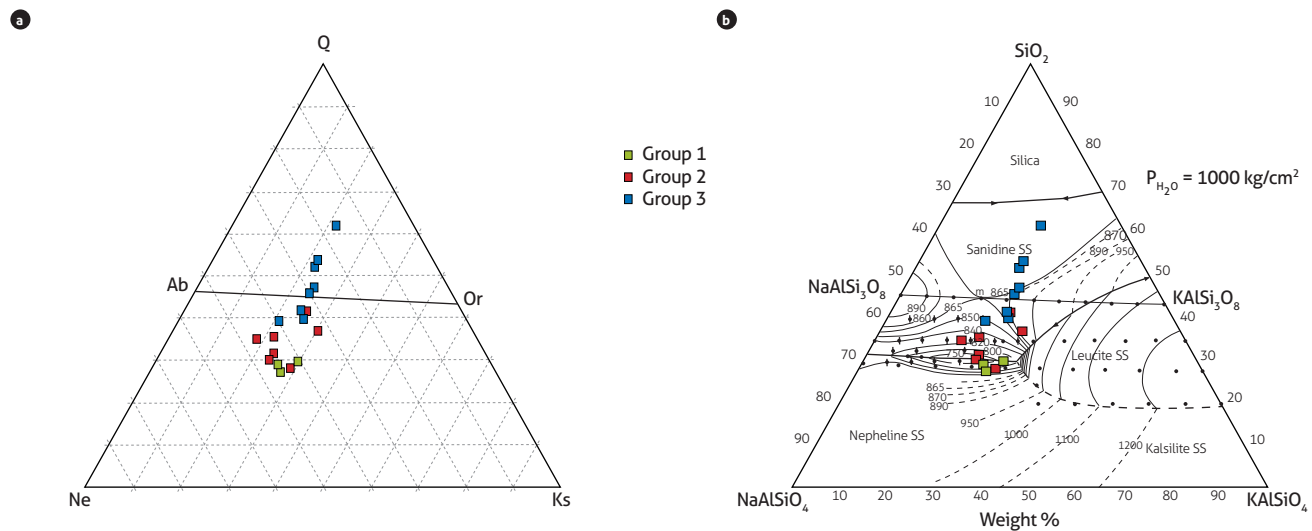


Figure 9. a) Rock composition in the Q-Ne-Ks system; b) Equilibrium phase diagram for the $NaAlSiO_4$ - $KAlSiO_4$ - SiO_2 system at 1 kbar. Source: adapted from Hamilton and Mackenzie (1965).

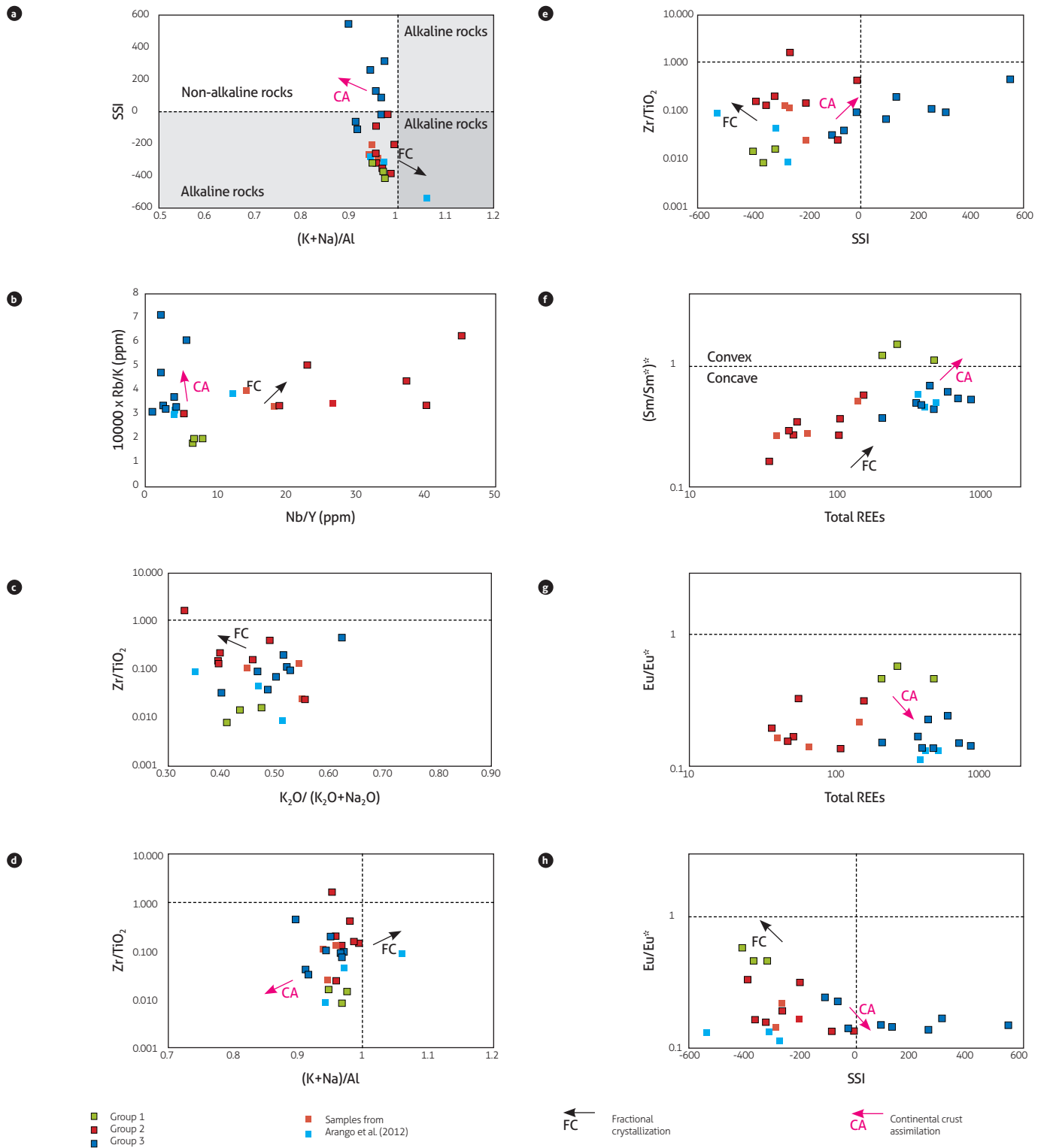


Figure 10. Compositional variation diagrams of SJGS rocks a) Silica saturation index (SSI) vs. (K+Na)/Al; b) Rb/K vs. Nb/Y; c) Zr/TiO₂ vs. K₂O/(K₂O+Na₂O); d) Zr/TiO₂ vs. (K+Na)/Al; e) Zr/TiO₂ vs. SSI; f) (Sm/Sm*)* vs. Total REE; g) Eu/Eu* vs. Total REE; h) Eu/Eu* vs. SSI. Source: adapted from Motoki et al. (2015). The diagram also shows data from Arango et al. (2012).

g, h, which show the effect of assimilation processes of the continental crust in addition to fractional crystallization processes. In the latter, the samples of groups 1 and 2 are connected by trends of fractional crystallization, albeit opposite to those observed in Figure 10b.

Field relationships showed the presence of metamorphic xenoliths partly absorbed in syenites in the southern section of the body. These xenoliths comprise rocks rich in SiO₂, which include the Si-saturated rocks of group 3. However, the relationship between the rocks of groups 2 and 3 is not limited to a simple assimilation model. The patterns observed in the diagrams presented by Motoki et al. (2010, 2015) indicate combined processes of fractional crystallization in groups 1 and 2 and assimilation in group 3.

In the Rb vs. (Y+Nb) tectonic discrimination diagram (Pearce et al., 1984), all rocks are placed in the within-plate granite (WPG) field (Figure 11), which corroborates the findings of other studies on the same unit, conducted north of the study area (Arango et al., 2011, 2012).

The comparison analysis of syenite rocks identified to the south and those to the north of SJGS reported in the study by Arango et al. (2011, 2012) shows that the compositional variation is higher in the southern SJGS rocks, which include nepheline syenites, syenites, and granites, whereas the northern SJGS rocks consist of only nepheline syenites (Figure 6).

In the multielement and REE diagrams (Figure 12), the northern SJGS (Arango et al., 2011, 2012) shows geochemical patterns similar to those of groups 2 and 3, defined for southern SJGS rocks; three samples show geochemical patterns similar to those of group 2, and the other three, to those of group 3. Sample 5000421 is deviates slightly from the pattern because it is impoverished in HREE relative to the group 3 field.

Although the composition of northern SJGS rocks is restricted to nepheline syenites, the main geochemical characteristics are similar to those of southern SJGS rocks, as are the concave-upward REE patterns, resulting from the impoverishment in MREE, slightly positive Eu anomaly, and positive Sr

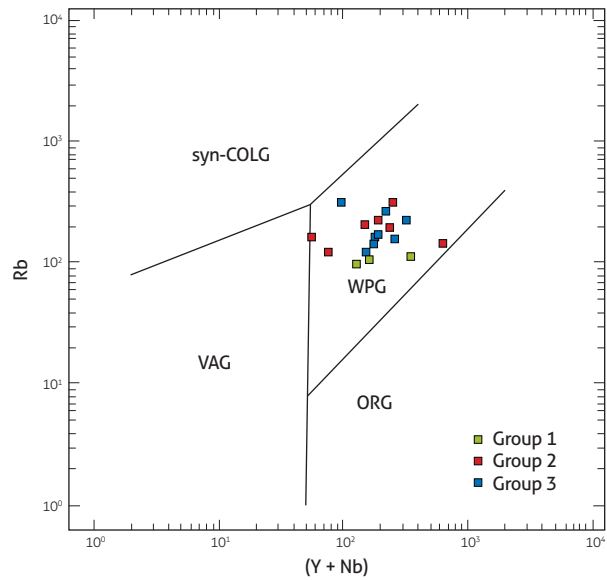


Figure 11. Tectonic discrimination diagram (Pearce et al., 1984) of the SJGS. The samples belong to the field of within-plate granites (WPG)

and Zr anomalies in group 2 and the relative enrichment in LREE in relation to the other groups, slightly negative Eu anomaly, and negative Sr and Zr anomalies in group 3.

4.4 Isotopes

The results from the Sm-Nd and Sr isotope analyses of two nepheline syenite (CAL-0014R, group 1, and JDB-0011R, group 2) and one syenogranite sample (JDB-0024R, Grupo 3) are outlined in Table 1. Based on geochronological data (Annex 3), a crystallization age of 604 Ma was used to calculate the $\epsilon_{Nd}(T)$ and the initial $^{87}Sr/^{86}Sr$ ratio of the samples.

The samples have positive values of $\epsilon_{Nd}(604)$, ranging from +0.8 to +1.8, with T_{DM} model ages ranging from 920 to 1000 Ma (Figure 13a). The ϵ_{Nd} values of the two nepheline syenite samples are very similar (+1.8 and +1.6) and slightly higher than that of the syenogranite sample (+0.6). In turn, the T_{DM} model ages of the nepheline syenite samples are consistent

Table 1. Sm-Nd and Sr isotopic data of the SJGS

Sample	Sm (ppm)	Nd (ppm)	¹⁴³ Nd/ ¹⁴⁴ Nd	¹⁴⁷ Sm/ ¹⁴⁴ Nd	$\epsilon_{Nd}(T)$	T_{DM} (Ga)	Rb (ppm)	Sr (ppm)	⁸⁷ Sr/ ⁸⁶ Sr	⁸⁷ Rb/ ⁸⁶ Sr	⁸⁷ Sr/ ⁸⁶ Sr _i	T (Ga)
CAL 0014R	15.77	100.06	0.512320 (±13)	0.0952	+1.6	0.93	113.5	4710.0	0.70536 (±1)	0.0699	0.70477	0.604
JDB-0011R	5.17	32.86	0.512329 (±17)	0.0952	+1.8	0.92	149.5	1220.0	0.70836 (±1)	0.3556	0.70536	0.604
JDB-0024R	14.44	90.41	0.512272 (±16)	0.0966	+0.6	1.00	157.5	249.0	0.72218 (±5)	1.8378	0.70665	0.604

The uncertainties in the last two digits of the ¹⁴³Nd/¹⁴⁴Nd ratios and in the last digit of the ⁸⁷Sr/⁸⁶Sr ratio are 2σ. The values of the ¹⁴³Nd/¹⁴⁴Nd_{CHUR} and ¹⁴⁷Sm/¹⁴⁴Nd_{CHUR} ratios used in the calculations were 0.512638 and 0.1966, respectively (Jacobsen and Wasserburg, 1980, 1984). T_{DM} model ages according to the depleted mantle model of DePaolo (1981). The concentrations of Rb and Sr were determined by ICP-MS analysis (Annex 1). The ⁸⁷Rb/⁸⁶Sr ratio was calculated according to the procedure described by Faure and Mensing (2005).

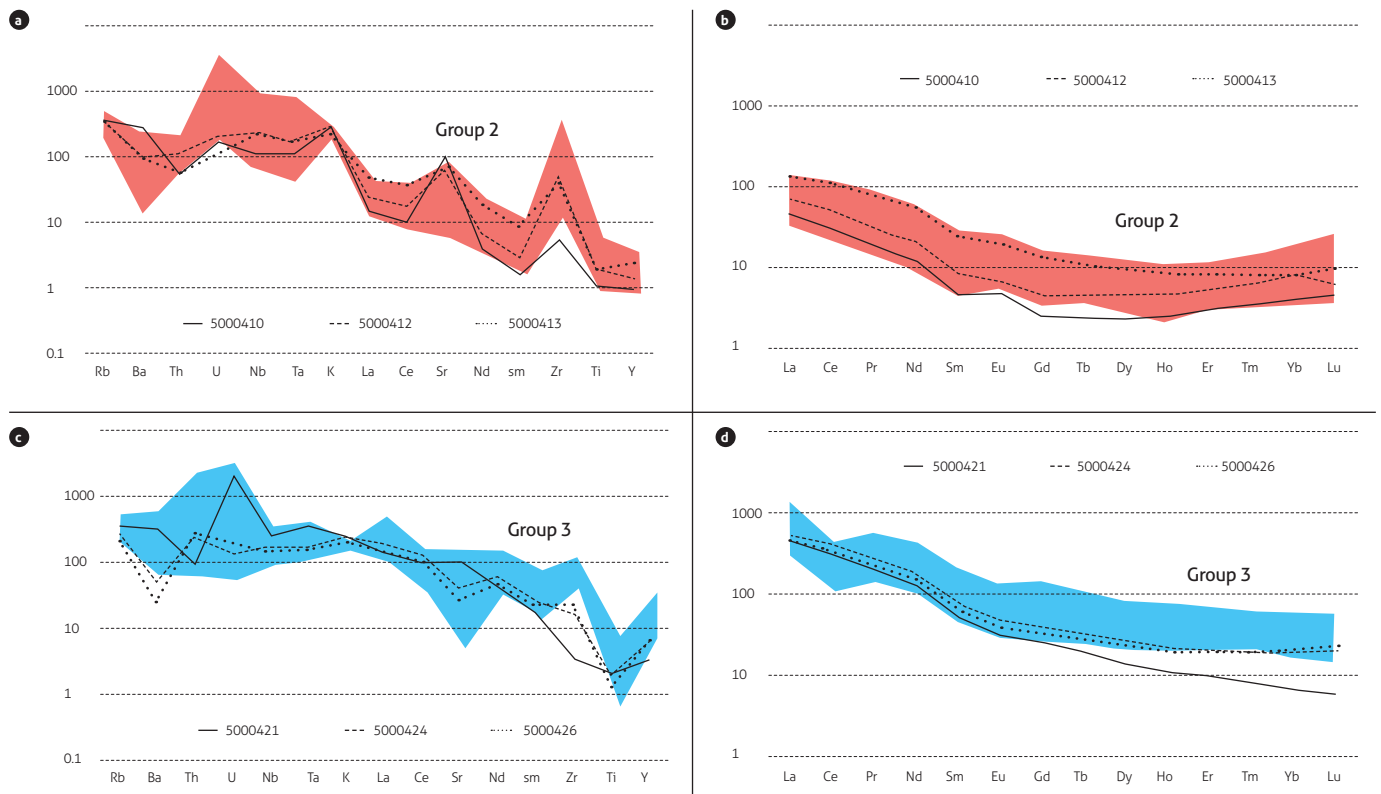


Figure 12. Primitive mantle- (McDonough et al., 1992) (a and b) and chondrite- (McDonough and Sun, 1995) (c and d) normalized multielement diagrams of northern (Arango et al., 2011, 2012) and southern SJGS rocks. The red and blue fields represent groups 2 and 3 defined in this study, respectively. The samples from the northern SJGS bodies are represented by lines.

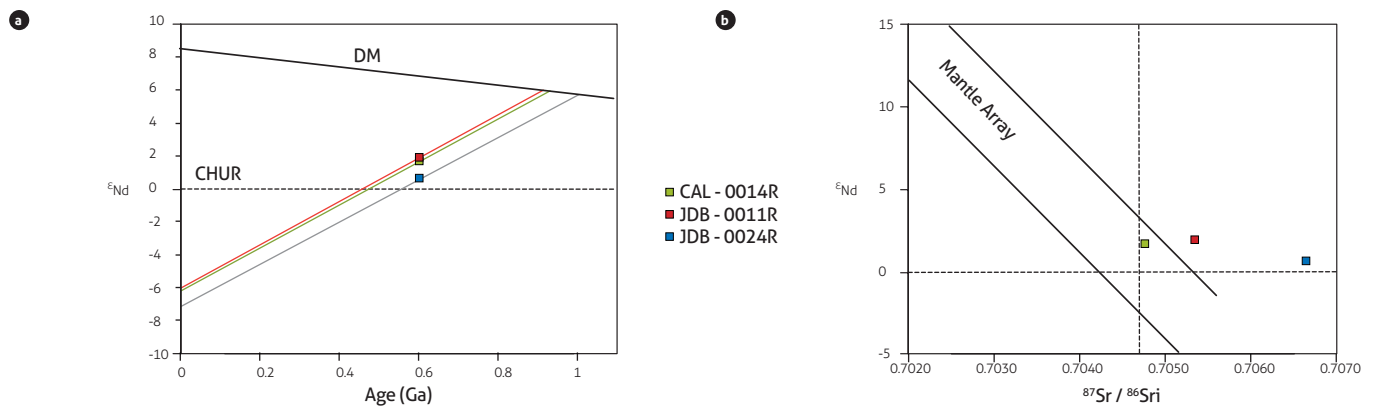


Figure 13. Isotope characteristics of the samples analyzed in this study a) ϵ_{Nd} vs. age chart showing the mantle-derived character of the rocks, for a magmatic crystallization age of 604 Ma; b) ϵ_{Nd} vs. $^{87}Sr/^{86}Sr$ chart showing isotope signatures ranging from typical mantle values to decoupled values with high initial $^{87}Sr/^{86}Sr$ ratios. Depleted mantle (DM) curve according to the model by DePaolo (1981).

(0.92 and 0.93 Ga), whereas the model age of the syenogranite sample is slightly older (1.0 Ga). With initial $^{87}\text{Sr}/^{86}\text{Sr}$ ratios ranging from 0.7048 to 0.7067, the isotope signatures of these samples range from those of typical mantle-derived magmas within the mantle array region until reaching decoupled signatures to the right of this field, characterized by high initial ratios of $^{87}\text{Sr}/^{86}\text{Sr}$ (Figure 13b). The latter is the case for the syenogranite sample, which has an initial $^{87}\text{Sr}/^{86}\text{Sr}$ ratio of 0.7067, whereas the nepheline syenite samples have lower ratios of 0.7048 and 0.7054.

4.5 Geochronology

Geochronological analyses were performed using the LA ICP-MS U-Pb zircon method in two syenite samples (Annex 3), one located in the El Capricho body (JDB-0001R) and the other located in the Cerrito body (OPP-0074R) (Figure 14).

Authors such as Pinson et al. (1962), Arango et al. (2011, 2012), Franco et al. (2018), and Muñoz Rocha et al. (2019) have reported ages ranging from the Ordovician to the Neoproterozoic for syenite rocks, calculated using different methods (Table 2). By K-Ar and Rb-Sr isotope dating of biotites,

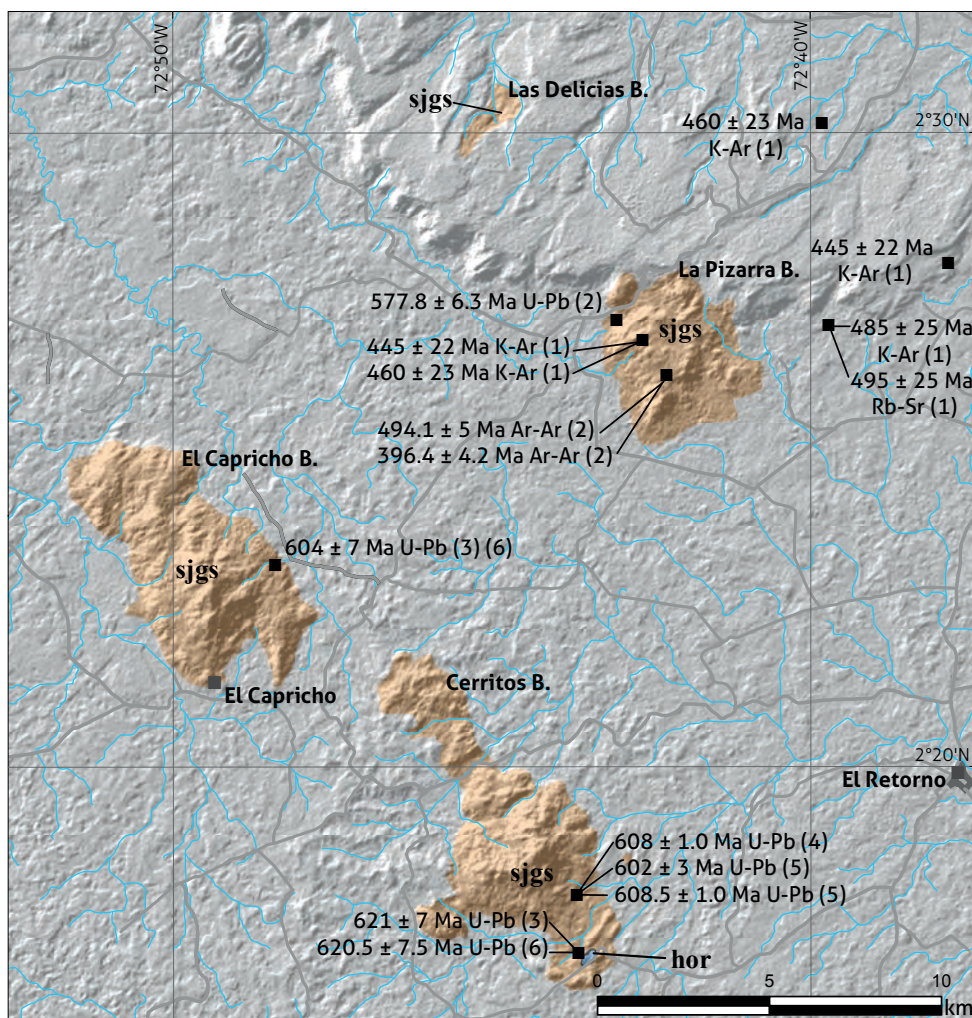


Figure 14. Ages of the different rock bodies that form the San José de Guaviare Syenite

Source: 1) Pinson et al. (1962); 2) Arango et al. (2011, 2012); 3) Maya et al. (2018); 4) Franco et al. (2018); 5) Muñoz Rocha et al. (2019); and 6) the present study.

Table 2. Ages of SJGS rocks assessed by different authors

Sample	Lithology	Reported age (Ma)	Recalculated age (Ma)	Method/material	Reference
B3592	Syenite	445 ± 22	457 ± 23	K-Ar/Biotite	(1) Pinson et al. (1962)
B3592	Syenite	460 ± 23	472 ± 24	K-Ar/biotite	(1) Pinson et al. (1962)
B3635	Syenite	445 ± 22	457 ± 23	K-Ar/biotite	(1) Pinson et al. (1962)
B3636	Syenite	460 ± 23	472 ± 24	K-Ar/biotite	(1) Pinson et al. (1962)
B3637	Syenite	485 ± 25	498 ± 26	K-Ar/biotite	(1) Pinson et al. (1962)
B3637	Syenite	495 ± 25	508 ± 26	Rb-Sr/biotite	(1) Pinson et al. (1962)
IGM500410	Nepheline syenite	494.1 ± 5		Ar-Ar/biotite	(2) Arango et al. (2011, 2012)
IGM500410	Nepheline syenite	396.4 ± 4.2		Ar-Ar/biotite	(2) Arango et al. (2011, 2012)
IGM500412	Nepheline syenite	577.8 ± 6.3		U-Pb/zircon	(2) Arango et al. (2012)
JDB-0001R (IGM5075537)	Nepheline syenite	604 ± 7		U-Pb/zircon	(3) Maya et al. (2018)
OPP-0074R (IGM5075695)	Syenite	621 ± 7		U-Pb/zircon	(3) Maya et al. (2018)
-	Nepheline syenite	608 ± 1		U-Pb/zircon	(4) Franco et al. (2018)
SNG-1	Nepheline syenite	602 ± 3		U-Pb/zircon	(5) Muñoz Rocha et al. (2019)
SNG-1	Nepheline syenite	608.5 ± 1.0		U-Pb/zircon	(5) Muñoz Rocha et al. (2019)
JDB-0001R (IGM5075537)	Nepheline syenite	604 ± 7		U-Pb/zircon	(6) Present study
OPP-0074R (IGM5075695)	Syenite	620.5 ± 7.5		U-Pb/zircon	(6) Present study

The ages calculated by Pinson et al. (1962) are corrected according to the constants of Steiger and Jager (1977) and to data published by Maya (1992).

Pinson et al. (1962) assessed ages ranging from 445 to 495 Ma for the La Pizarra body, which were considered ages of cooling by uplift followed by erosion or metamorphism, processes placed between the early and the Late Ordovician. A similar age of 494.1 ± 5 Ma, assessed in the same La Pizarra body using the $^{40}\text{Ar}/^{39}\text{Ar}$ biotite method, was reported by Arango et al. (2011, 2012). This age corresponds to the late Cambrian (Furongian) and was interpreted as a cooling age. Another age reported by Arango et al. (2011, 2012), using the U-Pb zircon method, is 577.8 ± 6.3-9 Ma (Ediacaran), which would be considered the age of crystallization. Other, more recent studies have yielded crystallization ages, assessed using the U-Pb zircon method, of 602 ± 3 and 608 ± 1 Ma (Ediacaran) for El Jordán syenite (Franco et al., 2018; Muñoz Rocha et al., 2019), which is found the southern section of the Cerritos body (Figure 14).

4.5.1 Nepheline syenite (JDB-0001R)

Zircons are in general anhedral and irregular, with a coarse concentric zoning of dark centers and lighter edges (Figure 15a, Annex 4). In dark zones, the uranium content is high, and the igneous fine oscillatory zoning is well defined. In contrast, in light zones, the uranium content is low, and the zoning is less perceptible or completely absent. The origin of this coarse zoning is not defined and could be associated with patchy zoning, attributed to local recrystallization along microfractures, according to Corfu et al. (2003). This characteristic is observed in one of the crystals with light veinlets that penetrate the dark zone

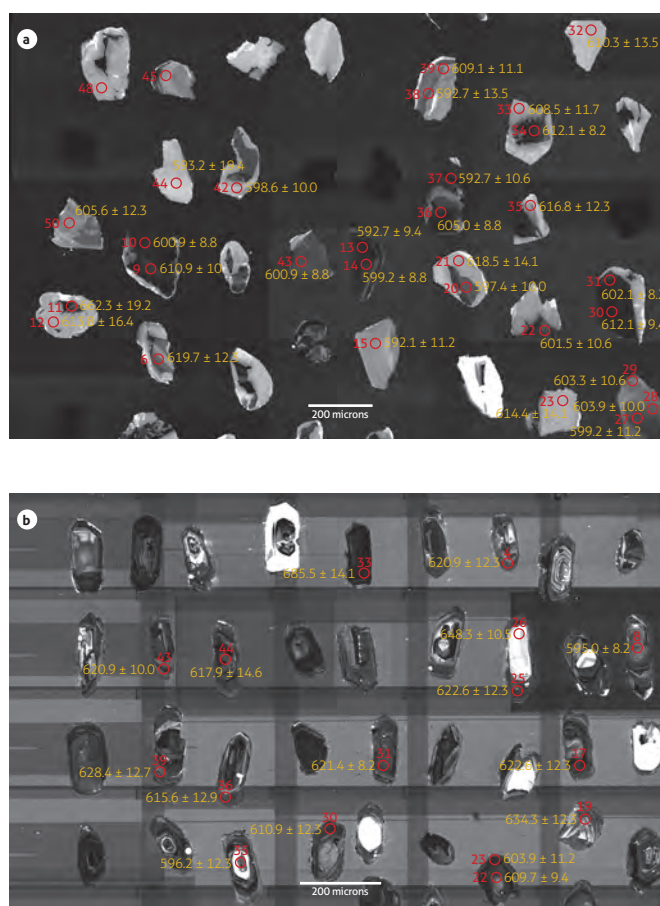


Figure 15. Cathodoluminescence images of SJGS zircons analyzed by LA-ICP-MS

a) Nepheline syenite (JDB-0001R); b) Syenite (OPP-0074R).

with good igneous fine zoning. The dark, uranium-rich areas may have begun to grow in a magma with a high content of this element, but the amount of uranium decreased due to assimilation of host rocks, as shown by the geochemical analysis.

The weighted-average $^{206}\text{Pb}/^{238}\text{U}$ age of this rock is $604.3 \pm 2.2/7.0$ Ma (2σ , $n=45$, $\text{MSWD}=1.6$), where the first level of uncertainty represents only internal analytical uncertainties, and the second level of uncertainty includes propagation from systematic and standard sources. This dating is interpreted as

the age of the magmatic event (Figure 16a) and corresponds to the Ediacaran period of the Neoproterozoic. The $^{206}\text{Pb}/^{238}\text{U}$ age that should be cited is 604 ± 7 Ma because this value was calculated considering all sources of uncertainty, both internal and systematic, as well as standardization. Two (inherited) zircon xenocrysts yielded individual $^{206}\text{Pb}/^{238}\text{U}$ ages of 647 ± 14 and 662 ± 19 Ma (Figure 16b, blue ellipses), and their ages support the assumption of a lengthy magmatism because the area shows no known igneous or late Neoproterozoic metamorphic events.

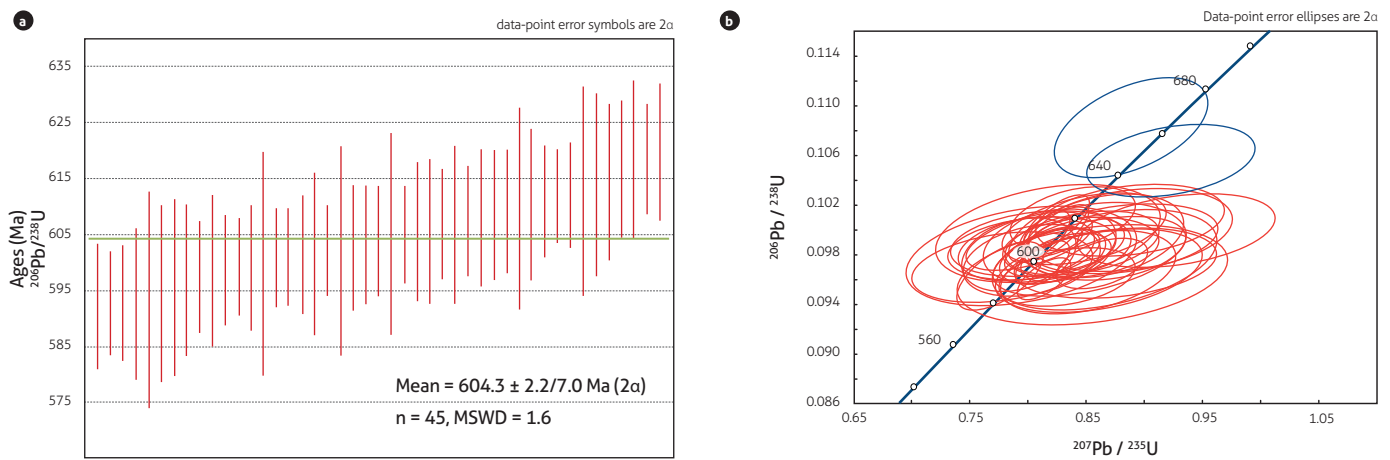


Figure 16. SJGS sample JDB-0001R
 a) Diagram of mean $^{206}\text{Pb}/^{238}\text{U}$ ages; b) 'Wetherill' concordia curve. Blue ellipses: inherited zircon ages.

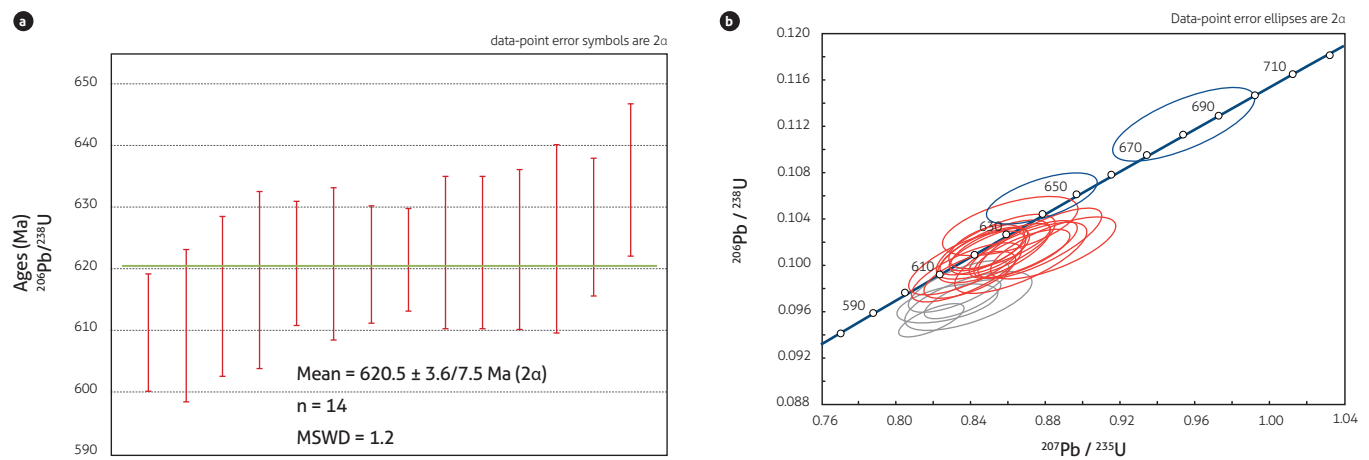


Figure 17. SJGS sample OPP-0074R
 a) Diagram of mean $^{206}\text{Pb}/^{238}\text{U}$ ages; b) 'Wetherill' concordia curve. Blue ellipses: inherited zircons ages; gray ellipses: zircons with likely Pb loss.

4.5.2 Syenite (OPP-0074R)

The zircons in this sample are euhedral and prismatic, with well-defined igneous oscillatory zoning along the grain boundaries, whereas cores with concentric, sectorial, and chaotic zoning, homogeneous light and dark textures, and inclusions are observed at the center in some crystals (Figure 15b, Annex 5). Other zircons have radial fractures, which are attributed to marked differences in uranium content within the zircon, according to Corfu et al. (2003).

The weighted-average $^{206}\text{Pb}/^{238}\text{U}$ ages of this sample is $620.5 \pm 3.6/7.5$ Ma (2σ , $n=14$, $\text{MSWD}=1.2$), which is interpreted as the crystallization age of this intrusive body during the Ediacaran (Figure 17a). For sample JDB-0001R, the $^{206}\text{Pb}/^{238}\text{U}$ age that should be cited is 620.5 ± 7.5 Ma, which includes all sources of uncertainty. Besides the zircons from the magmatic event, two inherited zircons yielded older $^{206}\text{Pb}/^{238}\text{U}$ ages of 648 ± 10 and 685 ± 15 Ma (Figure 17b). Four analyses with apparently younger $^{206}\text{Pb}/^{238}\text{U}$ ages are clearly discordant (gray ellipses in Figure 17b); these values are affected by Pb loss and were therefore disregarded when calculating the crystallization age of this sample.

5. DISCUSSION

The petrological evidence, the geochemical data, and the isotopic compositions of the nepheline syenite samples analyzed in this study (Figure 13b) indicate that the SJGS rocks derive from anorogenic and mantle-derived alkaline magmas subjected to magmatic differentiation and crustal assimilation.

Some of the magmas underwent fractional crystallization, resulting in Si-subsaturated compositions, which formed nepheline syenites. Others possibly reacted at the crustal level with the host rock, metamorphic rocks of the Guaviare Complex of varied compositions (Maya et al., 2018), producing some silica-saturated magmas, such as syenogranite. Such a contamination process is reflected in the isotope composition of a syenogranite sample, with an anomalously high initial $^{87}\text{Sr}/^{86}\text{Sr}$ ratio (0.7067, in contrast to the ratios of 0.7048 and 0.7054 of the nepheline syenite samples), which could have resulted from crustal assimilation of host rocks and/or rocks with low Rb/Sr ratios. Simultaneously, this contamination would also produce a lower ϵ_{Nd} value, assessed in syenogranite (+0.6), and an apparently older T_{DM} model age of 1000 Ma, in contrast to the model ages of 920 and 930 Ma assessed in the nepheline syenite samples. A similar origin has been suggested in other regions of the world where rocks

are simultaneously subsaturated and saturated in silica (Foland et al., 1993; Zhu et al., 2016).

U-Pb zircon ages reported by different authors, such as Arango et al. (2012), Franco et al. (2018), and Muñoz Rocha et al. (2019), and those assessed in this study indicate that syenite was intruded in the Ediacaran period of the Neoproterozoic, in a magmatic age range of at least 30 Ma, between $621 - 7$ and $577.8 + 6.3$ Ma, which would indicate that the syenite magmas were not all intruded simultaneously but rather that multiple intrusions occurred during that period. The samples dated in this study contain inherited zircons with a minimum age of $662.3-19.2$ Ma, that is, 643.1 Ma (Annex 3), and these zircons may be “antecrysts” formed in initial magma chambers of the syenites because no rocks of those ages are known in the area. Thus, the alkaline magmatism would have lasted approximately 59 million years. In the state of Bahia, Brazil, the alkaline magmatism associated with rifting lasted at least 58 million years (Rosa et al., 2007).

The Ar-Ar, K-Ar, and Rb-Sr biotite ages of intrusive rocks generally correspond to cooling ages. However, the large interval between the most recent U-Pb age (577.8 ± 6.3 Ma) and the oldest K-Ar age (508 ± 26 Ma) (Table 2) indicates a cooling age, below 300 °C, of 37 million years. Considering that hornfels were formed in the contact between syenite and regional metamorphic rocks, with injection migmatites, and not regional anatectic migmatites, the intrusion would have occurred at a depth of a few kilometers. Accordingly, cooling to 300 °C unlikely lasted 37 million years. Moreover, data presented by Arango et al. (2012) show that stepwise-extracted Ar fractions do not plateau well, which may result from excessive recoil during the $^{39}\text{K}(n,p)^{39}\text{Ar}$ reaction produced by irradiation, a complex thermal history, or the combination of both factors. The two possible events that may have generated a complex thermal history and that may have disturbed the K-Ar/ ^{40}Ar - ^{39}Ar systems are: 1) the Cambro-Ordovician sedimentary cover in the area may have been quite thick, which would have resulted in a complex cooling history of the syenites or allowed the syenites to reheat during tectonic burial; and 2) an important thermal event may have affected the western margin of the Amazonian Craton during the Cretaceous, as suggested by the presence of basaltic dikes dated at 102 Ma in the Araracuara region (Ibáñez-Mejía and Cordani, 2020). Although these rocks have not been reported in the Guaviare region, currently available data prevent us from ruling out the presence of a recent thermal event (for example, Cretaceous) in the area. Thus, the thermal and post-Ediacaran

tectonic burial history of the zone should be further studied to address these unanswered questions in the future.

The following model is proposed for the zone: At the end of the Neoproterozoic, a series of rifts enabled the disintegration of the Rodinia supercontinent into new continents. During this rifting period, at approximately 600 Ma, the northern zone of the Amazon was separated from Laurentia and Baltica, forming the Iapetus ocean (Condie, 2011; Cawood and Pisarevsky, 2017). Some of the rifts in the NW Amazon could have favored the intrusion of alkaline silica-subsaturated magmas, most likely generated by partial melting of mantle-derived igneous rocks during previous magmatic events, as indicated by the T_{DM} model ages of 920 and 930 Ma assessed in the nepheline syenite samples. These ages suggest that the source rocks of the SJGS magmas were likely formed during the Putumayo tectono-magmatic event, whose thermal and lithological record is common in several crustal segments of the northern Andes (Kroonenberg, 1982; Restrepo-Pace et al., 1997; Ramos, 2010; Cardona et al., 2010; Ibáñez-Mejía et al., 2011, 2015). Based on the isotope characteristics described in this study, an alternative origin of nepheline syenites related to juvenile mantle magmas (separated from the mantle at ~600 Ma) contaminated with older crust can also be ruled out; if such an origin were true, this contamination should have produced Si-saturated magmas, and therefore nepheline syenites would not have been formed in the first place, and their isotope signature would also be altered, moving away from the mantle array, as in the case of syenogranite.

Other authors have proposed different origins, such as crustal anatexis (Arango et al., 2011, 2012; Toussaint, 1993) or intraplate magmatism associated with Pan-African orogeny (Franco et al., 2018), which are not supported by isotope or regional geological data. Furthermore, Si-subsaturated magmas most likely cannot be derived from partial melting of common crustal rocks, which are typically saturated in quartz. Most data on alkaline magmatism reported in the literature indicate mantle sources with isotope signatures similar to those found in this study (Fitton and Upton, 1987; Winter, 2001).

6. CONCLUSIONS

U/Pb zircon dating of SJGS rocks places the unit in the Ediacaran, between 604 ± 7 and 620.5 ± 7.5 Ma. The SJGS derives from anorogenic magmatism in an intraplate setting, most likely resulting from rift-like stretching during the fragmenta-

tion of Rodinia at the end of the Neoproterozoic. The sources of the SJGS magmas would have been magmatic rocks directly formed by partial mantle melting during the Putumayo tectono-magmatic event.

The different syenite bodies consist of nepheline syenites, nepheline-bearing alkali-feldspar syenites, syenites, and syenogranites. The coexistence of nepheline- and quartz-bearing rocks could have resulted from the reaction between syenite magma and crustal rocks, which would have produced some silica-saturated magmas, such as the syenogranites that occur in southern SJGS bodies (El Capricho and Cerritos).

The southern SJGS syenite bodies tend to have broader compositions than the northern SJGS bodies, where the recorded rocks exclusively comprise nepheline syenites.

The SJGS is subdivided into three geochemical groups with contrasting characteristics that denote processes associated with the magmatic evolution of the igneous body, which include crustal differentiation and assimilation.

The intrusion of the SJGS generated a thermal metamorphism, in amphibolite and pyroxene-hornfels facies, in the host rocks of the Guaviare Complex, which allowed the recrystallization of minerals and the formation of hornfels and injection migmatites. A history of slow cooling, or a more recent thermal event not yet identified, affected the K-Ar/⁴⁰Ar-³⁹Ar systems of the syenites, yielding significantly younger ages than those assessed using the U-Pb zircon dating method.

ACKNOWLEDGEMENTS

This research summarizes and interprets part of the results from the project *Elaboración de la cartografía geológica en un conjunto de planchas a escala 1:100000 ubicadas en dos zonas del territorio colombiano, zona sur* [Geologic mapping of a set of plates at a 1:100 000 scale located in two zones of southern Colombia] of the Dirección de Geociencias Básicas del Servicio Geológico Colombiano (SGC), conducted by the geology team of the Serviminas company under contract No. 508 of 2017. Finally, the authors thank the anonymous reviewers for their valuable comments and suggestions, which helped to improve this manuscript.

SUPPLEMENTARY DATA

Supplementary data to this article can be found online at <https://doi.org/10.32685/0120-1425/bol.geol.48.1.2021.503>

REFERENCES

- Arango, M., Nivia, A., Zapata, G., Giraldo, M., Bermúdez, J., & Albarracín, H. (2011). *Geología y geoquímica de la Plancha 350 - San José del Guaviare. Memoria explicativa. Escala 1: 100.000*. Servicio Geológico Colombiano.
- Arango, M., Zapata, G., & Martens, U. (2012). Caracterización petrográfica, geoquímica y edad de la Sienita Nefelínica de San José del Guaviare. *Boletín de Geología*, 34(1), 15-26.
- Bowie, S., & Simpson, P. (1977). Microscopy: reflected light. In J. Zussman (ed.), *Physical methods in determinative mineralogy* (2nd ed., pp. 109-165). Academic Press, Ltd.
- Caicedo, J. C. (2003). *Toma de datos en la libreta de campo*. Ingeominas.
- Cardona, A., Chew, D., Valencia, V., Bayona, G., Mišković, A., & Ibáñez-Mejía, M. (2010). Grenvillian remnants in the Northern Andes: Rodinian and phanerozoic paleogeographic perspectives. *Journal of South American Earth Sciences*, 29(1), 92-104. <https://doi.org/10.1016/j.jsames.2009.07.011>
- Cawood, P., & Pisarevsky, S. (2017). Laurentia-Baltica-Ama-zonia relations during Rodinia assembly. *Precambrian Research*, 292, 386-397. <https://doi.org/10.1016/j.precamres.2017.01.031>
- Condie, K. (2011). The Supercontinent Cycle. In *Earth as an Evolving Planetary System* (pp. 317-355). Academic Press. <https://doi.org/10.1016/b978-0-12-385227-4.00003-1>
- Corfu, F., Hanchar, J., Hoskin, P., & Kinny, P. (2003). Atlas of zircon textures. *Reviews in Mineralogy and Geochemistry*, 53(1), 469-500. <https://doi.org/10.2113/0530469>
- Cox, K., Bell, J., & Pankhurst, R. (1979). *The interpretation of igneous rocks* (first ed.). Springer Science & Business Media. <https://doi.org/10.1007/978-94-017-3373-1>
- DePaolo, D. (1981). A neodymium and strontium isotopic study of the mesozoic calc-alkaline granitic batholiths of the Sierra Nevada and Peninsular Ranges, California. *Journal of Geophysical Research*, 86(B11), 10470-10488. <https://doi.org/10.1029/JB086iB11p10470>
- Faure, G., & Mensing, T. (2005). *Isotopes: principles and applications* (Third). John Wiley & Sons, Inc.
- Fitton, J., & Upton, B. (1987). Alkaline igneous rocks. *Geological Society Special Publication*, 30, 1-568.
- Foland, K., Landoll, J., Henderson, C., & Chen, J. (1993). Formation of cogenetic quartz and nepheline syenites. *Geochimica et Cosmochimica Acta*, 57(3), 697-704. [https://doi.org/10.1016/0016-7037\(93\)90380-F](https://doi.org/10.1016/0016-7037(93)90380-F)
- Franco, J., Muñoz, J., Piraquive, A., Bonilla, A., Amaya, Z., Cramer, T., & Campos, H. (2018). *Geochronology of the Nepheline Syenite of el Jordán, Guaviare Colombia, evidences of neoproterozoic-cambrian intraplate magmatism and its implications during Pan-African tectonics in western Gondwana*. EGU General Assembly Conference Abstracts. 10861.
- Galvis, J., Huguett, A., & Ruge, P. (1979). Geología de la Amazonia Colombiana. Informe No. 1792. *Boletín Geológico*, 22(3), 1-153.
- Gansser, A. (1954). The Guiana Shield (S. America). Geological observations. *Eclogae Geologicae Helveticae*, 47(1), 77-112.
- Gehrels, G., Valencia, V., & Ruiz, J. (2008). Enhanced precision, accuracy, efficiency, and spatial resolution of U-Pb ages by laser ablation-multicollector-inductively coupled plasma-mass spectrometry. *Geochemistry, Geophysics, Geosystems*, 9(3), 1-13. <http://doi.org/10.1029/2007GC001805>
- Gioia, S., Hollanda, M., & Pimentel, M. (1999). *Uso de resinas RE-Spec e Sr-Spec em geoquímica isotópica*. Anais do V congresso de geoquímica dos países de língua portuguesa e VII Congresso Brasileiro de Geoquímica. 218.
- Gioia, S., & Pimentel, M. (2000). The Sm-Nd isotopic method in the geochronology laboratory of the University of Brasília. *Anais da Academia Brasileira de Ciências*, 72(2), 219-245. <https://doi.org/10.1590/s0001-37652000000200009>
- Hamilton, D., & Mackenzie, W. (1965). Phase-equilibrium studies in the system NaAlSiO₄ (nepheline)-KAlSiO₄ (kalsilite)-SiO₂-H₂O. *Mineralogical Magazine and Journal of the Mineralogical Society*, 34(268), 214-231. <https://doi.org/10.1180/minmag.1965.034.268.17>
- Heinrich, E. (1965). *Microscopic identification of minerals*. McGraw-Hill.
- Ibáñez-Mejía, M., & Cordani, U. (2020). Zircon U-Pb geochronology and Hf-Nd-O isotope geochemistry of the Paleo- to Mesoproterozoic basement in the westernmost Guiana Shield (pp. 65-90). In Gómez, J. & Mateus-Zabala, D. (eds.), *The Geology of Colombia, Volume 1 Proterozoic - Paleozoic*. Publicaciones Geológicas Especiales 35, Servicio Geológico Colombiano. <https://doi.org/10.32685/pub.esp.35.2019.04>
- Ibáñez-Mejía, M., Pullen, A., Arenstein, J., Gehrels, G., Valley, J., Ducea, M., Mora, A., Pecha, M., & Ruiz, J. (2015). Unraveling crustal growth and reworking processes in complex zircons from orogenic lower-crust: the proterozoic Putumayo Orogen of Amazonia. *Precambrian Research*, 267, 285-310. <https://doi.org/10.1016/j.precamres.2015.06.014>

- Ibáñez-Mejía, M., Ruiz, J., Valencia, V., Cardona, A., Gehrels, G., & Mora, A. (2011). The Putumayo Orogen of Amazonia and its implications for Rodinia reconstructions: new U-Pb geochronological insights into the proterozoic tectonic evolution of northwestern South America. *Precambrian Research*, 191(1-2), 58-77. <https://doi.org/10.1016/j.precamres.2011.09.005>
- Ibáñez-Mejía, M., & Tissot, F. (2019). Extreme Zr stable isotope fractionation during magmatic fractional crystallization. *Science Advances*, 5(12), 1-14. <http://doi.org/10.1126/sciadv.aax8648>
- Jacobsen, S., & Wasserburg, G. (1980). Sm-Nd isotopic evolution of chondrites. *Earth and Planetary Science Letters*, 50(1), 139-155. [https://doi.org/10.1016/0012-821X\(80\)90125-9](https://doi.org/10.1016/0012-821X(80)90125-9)
- Jacobsen, S., & Wasserburg, G. (1984). Sm-Nd isotopic evolution of chondrites and achondrites, II. *Earth and Planetary Science Letters*, 67(2), 137-150. [https://doi.org/10.1016/0012-821X\(84\)90109-2](https://doi.org/10.1016/0012-821X(84)90109-2)
- Kroonenberg, S. (1982). A grenvillian granulite belt in the Colombian Andes and its relation to the Guiana Shield. *Geologie en Mijnbouw*, 61, 325-333.
- Lugmair, G., & Marti, K. (1978). Lunar initial $^{143}\text{Nd}/^{144}\text{Nd}$: differential evolution of the lunar crust and mantle. *Earth and Planetary Science Letters*, 39(3), 349-357. [https://doi.org/10.1016/0012-821X\(78\)90021-3](https://doi.org/10.1016/0012-821X(78)90021-3)
- Maniar, P., & Piccoli, P. (1989). Tectonic discrimination of granitoids. *Geological Society of America Bulletin*, 101(5), 635-643. [https://doi.org/10.1130/0016-7606\(1989\)101<0635:T-DOG>2.3.CO;2](https://doi.org/10.1130/0016-7606(1989)101<0635:T-DOG>2.3.CO;2)
- Maya, M. (1992). Catalogo de dataciones isotopicas en Colombia. *Boletín Geológico*, 32(1), 127-187.
- Maya, M., Amaya, C., Gómez, J., Tabares, G., Palacio, A., García, J., Tabares, F., Camacho, J., Betancur, J., & Duque, J. (2019). *Guía para la elaboración de la libreta de campo de un proyecto de cartografía geológica*. Serviminas.
- Maya, M., Amaya, C., Restrepo, J., Duque, J., Palacio, A., Gutiérrez, P., Pérez, O., Ríos, C., Arias, E., & Bedoya, J. (2018). *Memoria explicativa de la Plancha 372 – El Retorno. Escala 1: 100.000*. Servicio Geológico Colombiano.
- McDonough, W., & Sun, S. (1995). The composition of the earth. *Chemical Geology*, 120, 223-253.
- McDonough, W., Sun, S., Ringwood, A., Jagoutz, E., & Hofmann, A. (1992). Potassium, rubidium, and cesium in the earth and moon and the evolution of the mantle of the earth. *Geochimica et Cosmochimica Acta*, 56(3), 1001-1012. [https://doi.org/10.1016/0016-7037\(92\)90043-I](https://doi.org/10.1016/0016-7037(92)90043-I)
- Motoki, A., Sichel, S., Vargas, T., Aires, J., Iwanuch, W., Mello, S., Motoki, K., Silva, S., Balmant, A., & Gonçalves, J. (2010). Geochemical evolution of the felsic alkaline rocks of Tangará and Rio Bonito intrusive bodies, State of Rio de Janeiro, Brazil. *Geociências*, 29(3), 291-310.
- Motoki, A., Sichel, S., Vargas, T., Melo, D., & Motoki, K. (2015). Geochemical behaviour of trace elements during fractional crystallization and crustal assimilation of the felsic alkaline magmas of the state of Rio de Janeiro, Brazil. *Anais da Academia Brasileira de Ciências*, 87(4), 1959-1979. <https://doi.org/10.1590/0001-3765201520130385>
- Muñoz Rocha, J., Piraquive, A., Franco, J., Bonilla, A., Peña, M., Cramer, T., Rayo, L., & Villamizar, N. (2019). Megacircons ediacáricos de la Sienita Nefelínica de San José del Guaviare y su potencial como material de referencia para datación U/Pb mediante LA-ICP-MS. *Boletín Geológico*, 45, 5-22. <https://doi.org/10.32685/0120-1425/boletin-geo.45.2019.484>
- Nivia, A., Giraldo, M., Arango, M., Albarracín, H., Bermúdez, J., & Zapata, G. (2011). *Geología de la plancha 350 - San José del Guaviare - Mapa escala 1:100.000*. Servicio Geológico Colombiano.
- Pearce, J., Harris, N., & Tindle, A. (1984). Trace element discrimination diagrams for the tectonic interpretation of granitic rocks. *Journal of Petrology*, 25(4), 956-983. <https://doi.org/10.1093/petrology/25.4.956>
- Pinson, W., Hurley, P., Mencher, E., & Fairbairn, H. (1962). K-Ar and Rb-Sr ages of biotites from Colombia, South America. *GSA Bulletin*, 73(7), 907-910. [https://doi.org/10.1130/0016-7606\(1962\)73\[907:KARAOB\]2.0.CO;2](https://doi.org/10.1130/0016-7606(1962)73[907:KARAOB]2.0.CO;2)
- Pullen, A., Ibáñez-Mejía, M., Gehrels, G., Giesler, D., & Pecha, M. (2018). Optimization of a laser ablation-single collector-inductively coupled plasma-mass spectrometer (thermo element 2) for accurate, precise, and efficient zircon U-Th-Pb geochronology. *Geochemistry, Geophysics, Geosystems*, 19(10), 3689-3705. <http://doi.org/10.1029/2018GC007889>
- Ramos, V. (2010). The Grenville-age basement of the Andes. *Journal of South American Earth Sciences*, 29(1), 77-91. <https://doi.org/10.1016/j.jsames.2009.09.004>
- Restrepo-Pace, P., Ruiz, J., Gehrels, G., & Cosca, M. (1997). Geochronology and Nd isotopic data of Grenville-age rocks in the Colombian Andes: new constraints for late proterozoic-early paleozoic paleocontinental reconstructions of the Americas. *Earth and Planetary Science Letters*, 150(3-4), 427-441. [https://doi.org/10.1016/S0012-821X\(97\)00091-5](https://doi.org/10.1016/S0012-821X(97)00091-5)

- Rosa, M., Conceição, H., Macambira, M., Galarza, M., Cunha, M., Menezes, R., Marinho, M., Filho, B., & Rios, D. (2007). Neoproterozoic anorogenic magmatism in the Southern Bahia Alkaline Province of NE Brazil: U-Pb and Pb-Pb ages of the blue sodalite syenites. *Lithos*, 97(1-2), 88-97. <https://doi.org/10.1016/j.lithos.2006.12.011>
- Sláma, J., Košler, J., Condon, D., Crowley, J., Gerdes, A., Hanchar, J., Horstwood, M., Morris, G., Nasdala, L., Norberg, N., Schaltegger, U., Schoene, B., Tubrett, M., & Whitehouse, M. (2008). Plešovice zircon - A new natural reference material for U-Pb and Hf isotopic microanalysis. *Chemical Geology*, 249(1-2), 1-35. <http://doi.org/10.1016/j.chemgeo.2007.11.005>
- Steiger, R., & Jager, E. (1977). Subcommittee on geochronology: convention on the use of decay constants in geo- and cosmochronology. *Earth and Planetary Science Letters*, 36(3), 359-362. [https://doi.org/10.1016/0012-821X\(77\)90060-7](https://doi.org/10.1016/0012-821X(77)90060-7)
- Storey, M., Wolff, J., Norry, M., & Marriner, G. (1989). Origin of hybrid lavas from Agua de Pau volcano, Sao Miguel, Azores. *Geological Society of London, Special Publication*, 42, 161-180. <https://doi.org/https://doi.org/10.1144/GSL.SP.1989.042.01.11>
- Streckeisen, A. (1976). To each plutonic rock its proper name. *Earth Science Reviews*, 12(1), 1-33. [https://doi.org/10.1016/0012-8252\(76\)90052-0](https://doi.org/10.1016/0012-8252(76)90052-0)
- Toussaint, J. (1993). Introducción - Precámbrico. In *Evolución geológica de Colombia*. Universidad Nacional de Colombia.
- Trumpy, D. (1943). Pre-Cretaceous of Colombia. *GSA Bulletin*, 54(9), 1281-1304. <https://doi.org/10.1130/GSAB-54-1281>
- Trumpy, D. (1944). *El Precretaceo de Colombia*. Bogotá.
- Vesga, J., & Castillo, L. (1972). *Reconocimiento geológico y geoquímico preliminar del río Guaviare entre las confluencias con los ríos Ariari e Iteviare*. Ingeominas.
- Whitney, D., & Evans, B. (2010). Abbreviations for names of rock-forming minerals. *American Mineralogist*, 95(1), 185-187. <https://doi.org/10.2138/am.2010.3371>
- Winter, J. (2001). *An introduction to igneous and metamorphic petrology*. Prentice-Hall Inc.
- Wolff, J. (2017). On the syenite-trachyte problem. *Geology*, 45(12), 1067-1070. <https://doi.org/10.1130/G39415.1>
- Zhu, Y., Yang, J., Sun, J., Zhang, J., & Wu, F. (2016). Petrogenesis of coeval silica-saturated and silica-undersaturated alkaline rocks: mineralogical and geochemical evidence from the Saima alkaline complex, NE China. *Journal of Asian Earth Sciences*, 117, 184-207. <https://doi.org/10.1016/j.jseaes.2015.12.014>